Journal of Geochemical Exploration 161 (2016) 1–15

Contents lists available at ScienceDirect

Journal of Geochemical Exploration

journal homepage: www.elsevier.com/locate/jgeoexp

A new global database of δ^{98}Mo in molybdenites: A literature review and new data

N. Breillat [a,b,c,*], C. Guerrot [a,b,c], E. Marcoux [c], Ph. Négrel [a,b,c]

[a] BRGM, ISTO, UMR 7327, BP 36009, 45060 Orléans, France
[b] CNRS/INSU, ISTO, UMR 7327, 45071 Orléans, France
[c] University of Orléans, ISTO, UMR 7327, 45071 Orléans, France

ARTICLE INFO

Article history:
Received 1 August 2014
Revised 30 June 2015
Accepted 31 July 2015
Available online 10 September 2015

Keywords:
Molybdenum
Molybdenite
Isotopes
Mineralization

ABSTRACT

Isotopic compositions of Mo in molybdenites were used for deciphering a possible genetic link between isotopic variations and mineralizing processes, based on a worldwide molybdenite databank. We compared the $\delta^{98/95}$Mo (hereafter referred as $\delta^{98}Mo_{NIST}$) of 391 molybdenite samples (193 from the literature, 198 for this study) from different localities, different types of occurrences and different ages. The 198 molybdenite samples we analysed represent various types of mineralization in 6 granites, 11 pegmatites, 6 perigranitic veins, 2 greisen, 28 porphyry deposits, 5 skarns, 1 IOCG, and 9 Alpine-type fissure veins, with ages varying from 5 Ma to 2.7 Ga. The Mo isotopic composition was determined with an MC-ICP-MS Neptune after *aqua regia* dissolution and adjustment to $[Mo] = 1\ \mu g \cdot ml^{-1}$. Mass bias was corrected by using Zr as dopant and standard-sample-standard bracketing. The $\delta^{98}Mo_{NIST}$ ratios were normalized to NIST3134. External reproducibility is 0.07‰ (2σ). The overall range of the $\delta^{98}Mo_{NIST}$ ratio in the 391 molybdenite samples varied from −1.62 to 2.27‰, being higher for molybdenite formed in Alpine-type veins, greisen, perigranitic veins and IOCG, than for that in granite, pegmatite, porphyry deposits and skarns. The crystallization temperature can explain some of these differences, as polymetallic Alpine-type fissure veins broadly crystallize at lower temperatures than granite, pegmatite and porphyry deposits. For some occurrences the $\delta^{98}Mo_{NIST}$ was determined on several molybdenite samples, showing variability at occurrence scale. For example, in the Azegour skarn (Morocco) the $\delta^{98}Mo_{NIST}$ varies from −0.60 to 0.42‰ (n = 29), and in "Ravin de la Ruine" Alpine-type fissure veins (France) the variation is from −0.08 to 0.77‰ (n = 3). No correlation is seen between $\delta^{98}Mo_{NIST}$ and the age of the deposits.

1. Introduction

Over the past decades, the use of Mo-isotope compositions in the Earth Sciences has strongly increased, as well as that of other transition metals such as Fe, Cu, and Zn (Zhu et al., 2002). Mo-isotope applications were mainly developed for reconstructing paleo-redox conditions in oceans (Barling et al., 2001; Siebert et al., 2003; Arnold et al., 2004), and for investigating the main Mo input into oceans from weathering (Archer and Vance, 2008). More recently, Mo and other transition-metal isotopes were used for studying trace-metal pollution (Cu-Zn isotopes: Markl et al., 2006; Borrok et al., 2008; Mathur et al., 2013; Mo isotopes: Neubert et al., 2011; Chappaz et al., 2012; Lane et al., 2013). Molybdenum is used for alloying steel to increase strength and temperature resistance and for tinting. As molybdenite (MoS_2) is presently the only mineral source of Mo, it is important to study MoS_2 mineralizing processes.

Several studies have reported the Mo-isotope composition of ore deposits, particularly in order to constrain mineralizing processes (Hannah et al., 2007; Mathur et al., 2010; Greber et al., 2011, 2014; Shafiei et al., 2014). Understanding Mo-isotope fractionation processes during ore-deposit genesis is very important for understanding the mineralizing process as a whole. However, data normalization is problematic as each laboratory uses its own in-house standards, rendering inter-laboratory comparison of data sets difficult. Here, we used the NIST3134, recently proposed as the international δMo standard (Wen et al., 2010; Greber et al., 2012; Goldberg et al., 2013; Nägler et al., 2013) for homogenizing data sets of Mo isotopes in molybdenites, thus allowing the comparison of more than 391 data sets.

We discuss Mo-isotope ratios of 391 molybdenite samples from ore deposits all over the world and, for most samples, with a well understood geological context. The purpose of this study was twofold: (1) To investigate the isotopic variability of molybdenites from various geological settings covering a large time scale from Archean to "Recent" (<2 Ma); and (2) To investigate potential relationships between Mo-isotope variations and mineralizing processes. It is worth noting that samples from large Mo deposits, including Bugdaya (Kovalenker et al., 2011) and Zhireken (Berzina and Sotnikov, 2010) in Russia, Climax in the United States (Geraghty et al., 1988) and Chuquicamata in Chile (Ballard et al., 2001), or from newly discovered ones like Hashitu in China (Zhai et al.,

* Corresponding author at: BRGM, LAB/ISO, 3 avenue Claude Guillemin BP 6009, 45060 Orléans cedex 2, France.
E-mail address: noemie.breillat@gmail.com (N. Breillat).

http://dx.doi.org/10.1016/j.gexplo.2015.07.019
0375-6742/

2014) were analysed as part of this study. None of these major sites, of prime importance in terms of molybdenum reserves, have been analysed for molybdenum isotopic compositions.

2. The samples used for the databank

Deciphering the possible variations of Mo-isotope ratios in molybdenites, according to deposit type, geological context and age setting, requires the largest possible database. Thus, for this study we analysed 198 molybdenites for Mo isotopes, and, to complete our data set, we added all data from Barling et al. (2001), Siebert et al. (2001), Wieser and de Laeter (2003), Malinovsky et al. (2005, 2007), Hannah et al. (2007), Mathur et al. (2010), Greber et al. (2011, 2014), and Shafiei et al. (2014). These literature data used various different normalization standards and thus, to allow comparison, they were recalculated according to NIST3134 thanks to intercalibrations performed by Malinovsky et al. (2007), Goldberg et al. (2013) and Lane et al. (2013). The database now contains 391 data sets, including 193 molybdenite samples from the literature and 198 from our work. The samples have a world-wide provenance (Fig. 1); they were collected from ore deposits or came from various occurrences where the molybdenite content is not of economic interest. The types of molybdenite occurrences/deposits as well as studied sites and samples are described in Table 1.

3. Method

The first reliable isotope measurements for Mo were done by thermal-ionization mass spectrometry (TIMS) in the 1960s (Murthy, 1963) and improved regularly (Wieser and De Laeter, 2000) up to the development of the MC-ICP-MS method (Malinovsky et al., 2005). Molybdenite (molybdenum sulphide, MoS_2) is the main molybdenum ore. As Mo is the major cation in molybdenite (59.94%), there is no need for chemical purification and/or concentration prior to analysis (Barling et al., 2001).

Greber et al. (2011) found isotope variations within a single sample of molybdenite. Therefore, in order to obtain a representative value of the sample, the largest possible amount of molybdenite was handpicked and then powdered in order to homogenize the sample. Around 10 mg of molybdenite powder were dissolved in 4 ml of *aqua regia* (1 ml of HNO_3 7 N and 3 ml of HCl 8 N) at 100 °C in PTFE beakers until complete dissolution. The solutions were dried and the residues were dissolved in 10 ml of HNO_3 3% (*v*/*v*). From this concentrated solution, a final solution was prepared in HNO_3 3% in order to get a final Mo concentration of 1 $\mu g \cdot ml^{-1}$. Zr was added to this solution with a concentration of 0.5 $\mu g \cdot ml^{-1}$. The Mo blank level for the whole procedure was less than 1‰ and thus negligible as compared to the sample concentration.

Mo-isotopic measurements were done with an MC-ICP-MS Neptune (Thermo-Finnigan) at BRGM (Orléans, France), the experimental conditions being given in supplementary data. The MC-ICP-MS is preferred over TIMS for Mo-isotope studies since Lee and Halliday (1995) showed that the MC-ICP-MS instrument could produce precise and reproducible isotopic data for elements like Mo, that are difficult to ionize and measure with TIMS. The Neptune is a double-focusing mass spectrometer equipped with eight adjustable Faraday cups and one fixed axial cup, and skimmer cones H were used during this work. Zirconium (Zr) and ruthenium (Ru) produce several isobaric interferences on 92, 94, 96 and 96, 98, 100 masses, and only ^{95}Mo and ^{97}Mo are free of interference. Such interference is easily corrected with the following cup configuration: ^{90}Zr–L3, ^{91}Zr–L2, ^{92}Mo–^{92}Zr–L1, ^{94}Mo–^{94}Zr–Ax, ^{95}Mo–H1, ^{97}Mo–H2, ^{98}Mo–^{98}Ru–H3, ^{99}Ru–H4. In our samples and standards, ruthenium has never been detected. Mo-isotope measurements were run within sequences composed by blank, standard and sample analyses. After the sample and standard analyses, two minutes of washing (HNO_3 3%) allowed obtaining correct blanks. The reported data represent the mean value of a minimum of 5 runs of 20 measurements.

Mass bias was corrected by $^{90/91}$Zr external spiking (Zirconium ICP standard CertiPUR Merck) at 0.5 $\mu g \cdot ml^{-1}$ (Anbar et al., 2001) and standard-sample-standard bracketing. The external reproducibility

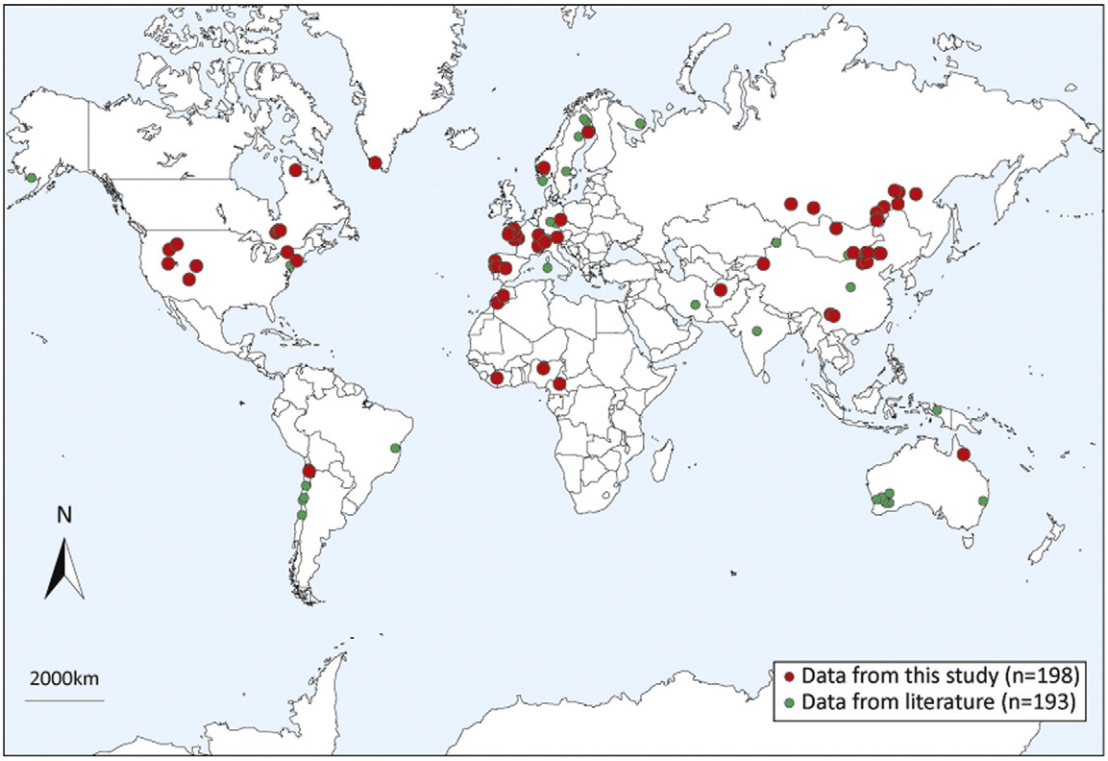

Fig. 1. Worldwide distribution of analysed molybdenite samples. Red points (n = 198) are data from this study and green points are data from the literature (n = 193).

Table 1
Description of the occurrences analysed in this study, including seven samples from six localities without enough information concerning the occurrence type or even the precise location, referred to hereafter as 'undefined'. References to sub samples are indicated by an additional subscript a to d, meaning up to 4 subsamples, i.e. same rock sample referred MoXXX and up to 4 samples of molybdenite grain in the samples MoXXX.

Occurrence type	T°C	ID	Location	Mineral assemblage	Age
Granite	<400–600 °C	Mo001	Kigom, Nigeria	Quartz vein with galena and silver	164 ± 4 Ma
		Mo031	Becon les granits, Maine-et-Loire, France		327–315 Ma
		Mo032	Becon les granits, Maine-et-Loire, France		327–315 Ma
		Mo033	Becon les granits, Maine-et-Loire, France		327–315 Ma
		Mo034	Becon les granits, Maine-et-Loire, France		327–315 Ma
		Mo053	Becon les granits, Maine-et-Loire, France		327–315 Ma
		Mo039	Man Departement, Ivory Coast	Pyroxene, molybdenite	Archean - Proterozoic
		Mo046	Bamiyan valley, Afghanistan		Upper Triassic to Liassic
		Mo047	Traouiéros, Côtes d'Armor, France		303 ± 15 Ma
		Mo167	Wurinitu, Inner Mongolia, China		120–140 Ma
		Mo168	Wurinitu, Inner Mongolia, China		120–140 Ma
		Mo169	Wurinitu, Inner Mongolia, China		120–140 Ma
		Mo170	Wurinitu, Inner Mongolia, China		120–140 Ma
		Mo171	Wurinitu, Inner Mongolia, China		120–140 Ma
Pegmatite	350–450 °C (London, 2009)	Mo002	Thornborough Hodgkinson Gold Field, Queensland, Australia		
		Mo009a	Preissac, Abitibi, Canada		2660–2681 Ma
		Mo009b	Preissac, Abitibi, Canada		2661–2681 Ma
		Mo010	Château-Lambert, Vosges, France		320–290 Ma
		Mo012	La clarté Ploumanac'h, Côtes d'Armor, France	Alcalin feldspars, plagioclase, quartz, biotite, molybdenite	303 ± 15 Ma
		Mo026	La clarté Ploumanac'h, Côtes d'Armor, France	Alcalin feldspars, plagioclase, quartz, biotite, molybdenite	303 ± 15 Ma
		Mo061	La clarté Ploumanac'h, Côtes d'Armor, France	Alcalin feldspars, plagioclase, quartz, biotite, molybdenite	303 ± 15 Ma
		Mo062	La clarté Ploumanac'h, Côtes d'Armor, France	Alcalin feldspars, plagioclase, quartz, biotite, molybdenite	303 ± 15 Ma
		Mo064	La clarté Ploumanac'h, Côtes d'Armor, France	Alcalin feldspars, plagioclase, quartz, biotite, molybdenite	303 ± 15 Ma
		Mo065	La clarté Ploumanac'h, Côtes d'Armor, France	Alcalin feldspars, plagioclase, quartz, biotite, molybdenite	303 ± 15 Ma
		Mo066	La clarté Ploumanac'h, Côtes d'Armor, France	Alcalin feldspars, plagioclase, quartz, biotite, molybdenite	303 ± 15 Ma
		Mo067	La clarté Ploumanac'h, Côtes d'Armor, France	Alcalin feldspars, plagioclase, quartz, biotite, molybdenite	303 ± 15 Ma
		Mo045	Nunavik, Québec, Canada	Micas, biotite, muscovite, molybdenite	
		Mo048	Menez Goaillou, France	Quartz, muscovite, molybdenite	320 Ma
		Mo049	Läven, Norway	Nepheline, arfvedsonite, lepidomelane, molybdenite, aegirine, magnetite with titanium	
		Mo050	Ivigtut, Arsuk, Greenland		1248 ± 25 Ma
		Mo051	Ivigtut, Arsuk, Greenland		1248 ± 25 Ma
		Mo052	Ivigtut, Arsuk, Greenland		1248 ± 25 Ma
		Mo069	Cubos e Chao do Castanheiro, Mangualde, Portugal		330–310 Ma
		Mo094	Sunderbyn, Luleå area, Sweden		
		Mo095	Sunderbyn, Luleå area, Sweden		
		Mo096	Sunderbyn, Luleå area, Sweden		
		Mo097	Sunderbyn, Luleå area, Sweden		
		Mo120a	Moly Hill mine, La Motte, Abitibi, Canada		Archean
		Mo120b	Moly Hill mine, La Motte, Abitibi, Canada		Archean
		Mo120c	Moly Hill mine, La Motte, Abitibi, Canada		Archean
		Mo121a	Moly Hill mine, La Motte, Abitibi, Canada		Archean
		Mo121b	Moly Hill mine, La Motte, Abitibi, Canada		Archean
		Mo121c	Moly Hill mine, La Motte, Abitibi, Canada		Archean
Perigranitic veins	374 °C	Mo025	Toul-Porz, Côtes du Nord, France	Molybdenite, quartz, scheelite, wolframite, chalcopyrite, bismuthinite	329 ± 5 Ma
		Mo028	Montbelleux-Luitré, Ile-et-Vilaine, France	Wolframite, molybdenite	490 ± 14 Ma
		Mo029	Villeray Parcé, Ille-et-Villaine, France	Quartz, molybdenite	490 ± 14 Ma
		Mo030	La Rousselière, Loire-Atlantique, France	Molybdenite, Bismuth	320–290 Ma
		Mo043	Tighza-Djebel Aouam, Morocco	Molybdenite, gold, scheelite	286 Ma
		Mo070	Salto do Lobo, Carris-Gerês, Portugal		330–310 Ma
Greisen	<300 °C (Fersman)	Mo027	Menez Gouaillou, Coray, Finistère, France	Molybdenite, arsenopyrite, bismuthinite	320 Ma
		Mo042	Altenberg, Germany		290–300 Ma
Mo-Porphyry deposit	<400–600 °C	Mo-Hend	Henderson mine, Colorado, USA		27.66 ± 10 Ma
		Mo-Hend-b	Henderson mine, Colorado, USA		27.66 ± 10 Ma
		Mo011	Henderson mine, Colorado, USA		27.66 ± 10 Ma
		Mo081	Climax, Colorado, USA		33–24 Ma
		Mo082	Climax, Colorado, USA		33–24 Ma

(continued on next page)

Table 1 (*continued*)

Occurrence type	T°C	ID	Location	Mineral assemblage	Age
Cu-Porphyry deposit	<400–600 °C	Mo054	Tilly, Québec, Canada		2745.8 ± 0.8 Ma
		Mo055	Tilly, Québec, Canada		2745.8 ± 0.8 Ma
		Mo056	Questa, New Mexico, USA		24 Ma
		Mo057	Questa, New Mexico, USA		24 Ma
		Mo079	Questa, New Mexico, USA		24 Ma
		Mo080	Questa, New Mexico, USA		24 Ma
		Mo058	Don-Rouyn, Abitibi, Canada		2700 Ma
		Mo059	Don-Rouyn, Abitibi, Canada		2700 Ma
		Mo063	Bingham Canyon, Utah, USA		38.55 ± 0.19 Ma
		Mo071	Chuquicamata, Chile		39.5–37.5 Ma
		Mo098	Tsagaan Suvarga, Omnogovi Province, Mongolia		240 Ma
		Mo099	Tsagaan Suvarga, Omnogovi Province, Mongolia		240 Ma
		Mo100	Hashitu, China		150 ± 4 Ma
		Mo101	Hashitu, China		150 ± 4 Ma
		Mo102	Hashitu, China		150 ± 4 Ma
		Mo103	Hashitu, China		150 ± 4 Ma
		Mo104	Hashitu, China		150 ± 4 Ma
		Mo105	Hashitu, China		150 ± 4 Ma
		Mo106	Hashitu, China		150 ± 4 Ma
		Mo107	Hashitu, China		150 ± 4 Ma
		Mo108	Hashitu, China		150 ± 4 Ma
		Mo109	Thompson Creek, Idaho, USA		
		Mo110	Thompson Creek, Idaho, USA		
		Mo111	Butte, Montana, USA		62.8 Ma
		Mo112	Butte, Montana, USA		62.8 Ma
		Mo113	Butte, Montana, USA		62.8 Ma
		Mo114	Butte, Montana, USA		62.8 Ma
		Mo115	Butte, Montana, USA		62.8 Ma
		Mo116	Butte, Montana, USA		62.8 Ma
		Mo117	Butte, Montana, USA		62.8 Ma
		Mo118	Butte, Montana, USA		62.8 Ma
		Mo119	Butte, Montana, USA		62.8 Ma
		Mo122	Sora, Russia	Quartz-molybdenite vein	405–388 Ma
		Mo123	Sora, Russia	Molybdenite nests in K-feldspar metasomatite	405–388 Ma
		Mo124	Sora, Russia	Molybdenite dissemination in syenite	405–388 Ma
		Mo125	Sora, Russia	Molybdenite dissemination in quartz cement from breccia ore zone	405–388 Ma
		Mo126	Zhireken, Eastern Transbaikalia, Russia	Coarse-grained molybdenite in quartz vein	160–155 Ma
		Mo127	Zhireken, Eastern Transbaikalia, Russia	Molybdenite dissemination in granite	160–155 Ma
		Mo128	Zhireken, Eastern Transbaikalia, Russia	Molybdenite disseminated in quartz-K-feldspar metasomatite	160–155 Ma
		Mo129	Zhireken, Eastern Transbaikalia, Russia	Nests of molybdenite in altered fine-grained granites (argillic alteration)	160–155 Ma
		Mo130	Zhireken, Eastern Transbaikalia, Russia	Nests of molybdenite in potassically altered granites	160–155 Ma
		Mo131	Zhireken, Eastern Transbaikalia, Russia	Quartz-molybdenite veinlets	160–155 Ma
		Mo132	Zhireken, Eastern Transbaikalia, Russia	Molydenite from breccia of argillized fine-grained granites (molybdenite composing cement of this breccia)	160–155 Ma
		Mo133	Aksug, Russia	Molybdenite veinlet in tonalite	404–401 Ma
		Mo134	Aksug, Russia	Molybdenite dissemination in potassically altered granodiorite porphyry	404–401 Ma
		Mo135	Shaktama, Eastern Transbaikalia, Russia	Molybdenite veinlet in granite	155–150 Ma
		Mo136	Shaktama, Eastern Transbaikalia, Russia	Molybdenite-pyrite vein in altered granite	155–150 Ma
		Mo137	Shaktama, Eastern Transbaikalia, Russia	Quartz-molybdenite veinlet	155–150 Ma
		Mo138	Erdenetuin Ovoo, Mongolia	Quartz-molybdenite-pyrite veinlets in granodiorite porphyry	240–220 Ma
		Mo139	Erdenetiin Ovoo, Mongolia	Quartz-molybdenite veinlet	240–220 Ma
		Mo140	Erdenetiin Ovoo, Mongolia	Molybdenite from quartz-sericite metasomatite	240–220 Ma
		Mo141	Bugdaya, Eastern Transbaikalia, Russia	Molybdenite veinlet in altered quartz porphyry (quartz-albite alteration)	154 ± 3 Ma
		Mo149	Bugdaya, Eastern Transbaikalia, Russia		154 ± 3 Ma
		Mo150	Bugdaya, Eastern Transbaikalia, Russia		154 ± 3 Ma
		Mo151	Bugdaya, Eastern Transbaikalia, Russia		154 ± 3 Ma
		Mo152	Bugdaya, Eastern Transbaikalia, Russia		154 ± 3 Ma
		Mo153	Bugdaya, Eastern Transbaikalia, Russia		154 ± 3 Ma
		Mo142	Davenda, Eastern Transbaikalia, Russia	Quartz-molybdenite vein	Mesozoic
		Mo143	Davenda, Eastern Transbaikalia, Russia	Quartz-molybdenite veinlet in aplite-like granite	Mesozoic
		Mo144	Davenda, Eastern Transbaikalia, Russia	Quartz-molybdenite veinlet in potassically altered granite	Mesozoic
		Mo145	Chubachi, Russia	Quartz-molybdenite veinlet in granodiorite porphyry	130 Ma
		Mo146	Veseloye, Russia	Quartz-molybdenite-pyrite vein in granite	
		Mo147	Okonon, Russia	Quartz-molybdenite-pyrite veinlet in granodiorite porphyry	

Table 1 (*continued*)

Occurrence type	T°C	ID	Location	Mineral assemblage	Age
		Mo148	Vykhodnoye, Russia	Quartz-molybdenite veinlet in granodiorite porphyry	110–105 Ma
		Mo154	Dasuji-Zhuozi county, Inner Mongolia, China		120–140 Ma
		Mo155	Caosiyao-Xinghe county, Inner Mongolia, China		120–140 Ma
		Mo156	Caosiyao-Xinghe county, Inner Mongolia, China		120–140 Ma
		Mo157	Caosiyao-Xinghe county, Inner Mongolia, China		120–140 Ma
		Mo158	Caosiyao-Xinghe county, Inner Mongolia, China		120–140 Ma
		Mo159	Caosiyao-Xinghe county, Inner Mongolia, China		120–140 Ma
		Mo160	Caosiyao-Xinghe county, Inner Mongolia, China		120–140 Ma
		Mo161	Caosiyao-Xinghe county, Inner Mongolia, China		120–140 Ma
		Mo162	Ulandler-Sunid Zuoqi area, Inner Mongolia, China		120–140 Ma
		Mo163	Ulandler-Sunid Zuoqi area, Inner Mongolia, China		120–140 Ma
		Mo164	Ulandler-Sunid Zuoqi area, Inner Mongolia, China		120–140 Ma
		Mo165	Ulandler-Sunid Zuoqi area, Inner Mongolia, China		120–140 Ma
		Mo166	Ulandler-Sunid Zuoqi area, Inner Mongolia, China		120–140 Ma
		Mo172	Donggebi, Tianshan, China		235 Ma
		Mo173	Dongchuan, Yunnan, China	Molybdenite-mineralized albitite, disseminate	1–1.2 Ga
		Mo174	Linxi, Inner Mongolia, China	Dark grey silty tuffaceous slate with molybdenite veinlet and quartz vein	120–140 Ma
		Mo175	Linxi, Inner Mongolia, China	Hoar altered rocks with molybdenite veinlet, disseminated molybdenite, and quartz vein	120–140 Ma
		Mo176	Donggebi, Tianshan, China		235 Ma
		Mo177	Donggebi, Tianshan, China		235 Ma
		Mo178	Donggebi, Tianshan, China		235 Ma
		Mo179	Donggebi, Tianshan, China		235 Ma
Skarn	200–1200 °C (Wallmach et al., 1989)	Mo004	Azegour, Morocco	Coarse molybdenite in grenatite, few micrograins of chalcopyrite	271 ± 3 Ma
		Mo007	Azegour, Morocco	Coarse molybdenite in grenatite, few micrograins of chalcopyrite	271 ± 3 Ma
		Mo008	Azegour, Morocco	Coarse molybdenite in grenatite, few micrograins of chalcopyrite	271 ± 3 Ma
		Mo072	Azegour, Morocco	Coarse molybdenite in grenatite, few micrograins of chalcopyrite	271 ± 3 Ma
		Mo073	Azegour, Morocco	Coarse molybdenite in grenatite, few micrograins of chalcopyrite	271 ± 3 Ma
		Mo074a	Azegour, Morocco	Coarse molybdenite in grenatite, few micrograins of chalcopyrite	271 ± 3 Ma
		Mo074b	Azegour, Morocco	Coarse molybdenite in grenatite, few micrograins of chalcopyrite	271 ± 3 Ma
		Mo074c	Azegour, Morocco	Coarse molybdenite in grenatite, few micrograins of chalcopyrite	271 ± 3 Ma
		Mo075a	Azegour, Morocco	Coarse molybdenite in grenatite, few micrograins of chalcopyrite	271 ± 3 Ma
		Mo075b	Azegour, Morocco	Coarse molybdenite in grenatite, few micrograins of chalcopyrite	271 ± 3 Ma
		Mo076a	Azegour, Morocco	Coarse molybdenite in grenatite, few micrograins of chalcopyrite	271 ± 3 Ma
		Mo076b	Azegour, Morocco	Coarse molybdenite in grenatite, few micrograins of chalcopyrite	271 ± 3 Ma
		Mo077	Azegour, Morocco	Disseminate molybdenite in grenatite	271 ± 3 Ma
		Mo078	Azegour, Morocco	Disseminate molybdenite in grenatite	271 ± 3 Ma
		Mo084a	Azegour, Morocco	Coarse molybdenite in grenatite, few micrograins of chalcopyrite	271 ± 3 Ma
		Mo084b	Azegour, Morocco	Coarse molybdenite in grenatite, few micrograins of chalcopyrite	271 ± 3 Ma
		Mo084c	Azegour, Morocco	Coarse molybdenite in grenatite, few micrograins of chalcopyrite	271 ± 3 Ma
		Mo085a	Azegour, Morocco	Coarse molybdenite in grenatite, few micrograins of chalcopyrite	271 ± 3 Ma
		Mo085b	Azegour, Morocco	Coarse molybdenite in grenatite, few micrograins of chalcopyrite	271 ± 3 Ma
		Mo085c	Azegour, Morocco	Coarse molybdenite in grenatite, few micrograins of chalcopyrite	271 ± 3 Ma
		Mo085d	Azegour, Morocco	Coarse molybdenite in grenatite, few micrograins of chalcopyrite	271 ± 3 Ma
		Mo086a	Azegour, Morocco	Coarse molybdenite in grenatite, few micrograins of chalcopyrite	271 ± 3 Ma
		Mo086b	Azegour, Morocco	Coarse molybdenite in grenatite, few micrograins of chalcopyrite	271 ± 3 Ma
		Mo087	Azegour, Morocco	Coarse molybdenite in grenatite, few micrograins of chalcopyrite	271 ± 3 Ma
		Mo088a	Azegour, Morocco	Coarse molybdenite in grenatite, few micrograins of chalcopyrite	271 ± 3 Ma
		Mo088b	Azegour, Morocco	Coarse molybdenite in grenatite, few micrograins of chalcopyrite	271 ± 3 Ma

(*continued on next page*)

Table 1 (*continued*)

Occurrence type	T°C	ID	Location	Mineral assemblage	Age
Skarn	200–1200 °C (Wallmach et al., 1989)	Mo089a	Azegour, Morocco	Coarse molybdenite in grenatite, few micrograins of chalcopyrite	271 ± 3 Ma
		Mo089b	Azegour, Morocco	Coarse molybdenite in grenatite, few micrograins of chalcopyrite	271 ± 3 Ma
		Mo090	Azegour, Morocco	Coarse molybdenite in grenatite, few micrograins of chalcopyrite	271 ± 3 Ma
		Mo035	Dielette-Flamanville, Manche, France		320 Ma
		Mo036	Dielette-Flamanville, Manche, France		320 Ma
		Mo040	Isk Imoula, Tichka, Morocco		Late hercynian
		Mo041	Ikissane, Tichka, Morocco	Molybdenite, copper	Late hercynian
		Mo083	Edwards, New York, USA		1100 Ma
Alpine-type fissure veins	<300 °C	Mo013	La Meije, Hautes Alpes, France		23–5 Ma
		Mo014	Combe Laurichard, Hautes Alpes, France		23–5 Ma
		Mo015	Glacier de l'homme,Hautes Alpes, France		23–5 Ma
		Mo016	Clos l'Oureou, Hautes Alpes, France		23–5 Ma
		Mo017	Clos l'Oureou, Hautes Alpes, France		23–5 Ma
		Mo018	Glacier de Bonne Pierre, Isère, France		23–5 Ma
		Mo019	Glacier de Bonne Pierre, Isère, France		23–5 Ma
		Mo020	Glacier de Bonne Pierre, Isère, France		23–5 Ma
		Mo021	Ravin de la Ruine, Isère, France		23–5 Ma
		Mo022	Ravin de la Ruine, Isère, France		23–5 Ma
		Mo023	Ravin de la Ruine, Isère, France		23–5 Ma
		Mo024	Tête du Rouget, Isère, France		23–5 Ma
		Mo037	Baltschiedertal, Switzerland		23–5 Ma
		Mo038	Baltschiedertal, Switzerland		23–5 Ma
		Mo060	Stilluptal, Zillertal, Austria	Albite, chlorite, muscovite, quartz, molybdenite	23–5 Ma
IOCG	160–800 °C (Chen, 2008)	Mo091	Lala, China		1086 ± 8 Ma
Unknown origin		Mo003	Spain		
		Mo005	Morocco		
		Mo006	Québec, Canada		
		Mo044	Cameroon	Marble, serpentine, molybdenite	
		Mo068	Borralha, Portugal		320 Ma
		Mo092	Sunderbyn, Luleå area, Sweden		
		Mo093	Sunderbyn, Luleå area, Sweden		

obtained was 0.06‰ and 0.08‰ (2σ, n = 137) for $\delta^{97/95}$Mo (here referred as δ^{97}Mo) and δ^{98}Mo, respectively, on an ICP internal standard solution (Techlab n°B3015042) (Fig. 2a). The reproducibility was 0.05‰ and 0.08‰ (2σ, n = 85) for δ^{97}Mo and δ^{98}Mo, respectively, on a molybdenite matrix (Fig. 2b), corresponding to repeated analyses of the Henderson molybdenite (Reference Material 8599 for Re-Os, Markey et al., 2007). Both are equal to the reproducibility obtained in recent work on Mo-isotope analyses on molybdenites (e.g. Greber et al., 2014).

All data are reported as classic δ^{98}Mo units relative to a standard solution according to the following formula:

$$\delta^{98}\mathrm{Mo} = \left[\frac{(98\mathrm{Mo}/95\mathrm{Mo})_{sample}}{(98\mathrm{Mo}/95\mathrm{Mo})_{standard}} - 1\right] * 1000. \quad (1)$$

Today, there is no internationally accepted standard and, in order to report our data in δ-units, we used the NIST3134 solution (lot#891307), which has been proposed as a reference for reporting Mo-isotopic compositions (Wen et al., 2010; Greber et al., 2012; Goldberg et al., 2013; Nägler et al., 2013). Data are often reported as δ^{97}Mo, which is related to δ^{98}Mo by the relation: $\delta^{97}\mathrm{Mo} = \frac{2}{3}\,\delta^{98}\mathrm{Mo}$ (Anbar, 2004). We tested the mean of δ^{97}Mo versus δ^{98}Mo for all samples analysed for this study, the mean values for Henderson molybdenite (n = 85, −0.13 ± 0.05 and −0.20 ± 0.08‰ for δ^{97}Mo and δ^{98}Mo, respectively) and the ICP internal standard solution (n = 137, −0.16 ± 0.06 and −0.24 ± 0.08‰ for δ^{97}Mo and δ^{98}Mo, respectively). The relationship obtained gave a graphical slope of the fractionation line at 1.480 ± 0.004, in full agreement with the expected value of 1.5, demonstrating the validity of our corrections (see supplementary material).

Furthermore, four eluted fractions of a Sigma-Aldrich Mo solution as described in Wen et al. (2010) —who proposed such fractionated Mo solutions as secondary reference materials— were analysed by three laboratories (ENS-Lyon and CRPG Nancy in France, and LISG-MLR in China). During this study, we obtained mean $\delta^{98}\mathrm{Mo}_{NIST}$ values of 3.46 ± 0.06‰ (n = 30), 1.57 ± 0.08‰ (n = 33), −1.67 ± 0.06‰ (n = 33), −2.81 ± 0.06‰ (n = 32), respectively for solutions 1, 2, 3 and 4. The $\delta^{98}\mathrm{Mo}_{NIST}$ mean values cited in Wen et al. (2010) are respectively 3.24 ± 0.35‰, 1.42 ± 0.41‰, −1.63 ± 0.29‰ and −2.88 ± 0.32‰ for the same solutions. Our results agree well with the measurements made in the three other laboratories (Fig. 3). Hereafter, the δ^{98}Mo calculated following Eq. (1), where the NIST3134 is used as standard is referred to as $\delta^{98}\mathrm{Mo}_{NIST}$.

4. Results and discussion

For this study, 198 molybdenites were analysed and the results are listed in Table 2. The following statistical analysis is based on our data (Table 2) and supplementary data from the literature (n = 193; see Table 2 in supplementary data). All data were converted to the NIST3134 standard in order to create internally consistent database. Unfortunately, data from Pietruszka et al. (2006) are could not be included because of a lack of intercalibration of their standard.

4.1. $\delta^{98}Mo_{NIST}$ variations and occurrence types

Fig. 4 illustrates the distribution of $\delta^{98}\mathrm{Mo}_{NIST}$ values for all data in our database, in addition with their discrimination according to the ten discriminated types of molybdenite occurrences/deposits; note that $\delta^{98}\mathrm{Mo}_{NIST}$ vary greatly from −1.62 to 2.27‰. For the main occurrence/deposit types, variations around 2‰ for the Mo isotopes can be seen in pegmatites, skarns or porphyry deposits, up to 2.6‰ for greisen and granites.

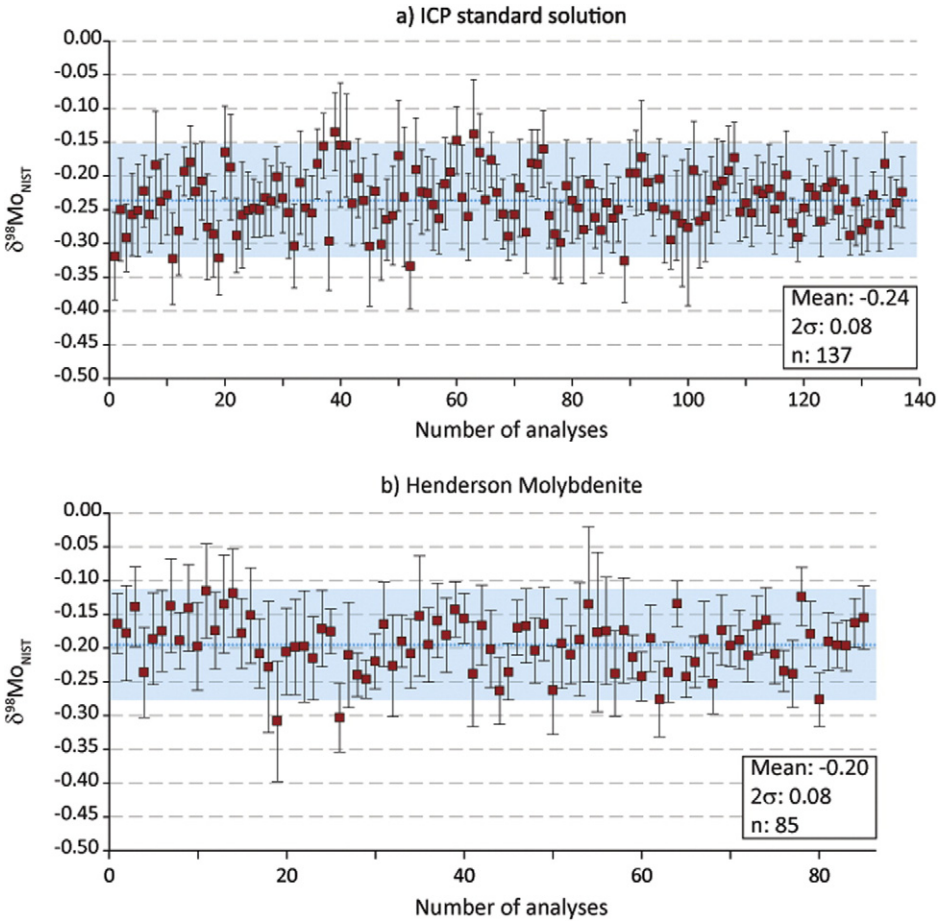

Fig. 2. Long-term reproducibility of the δ^{98}Mo: a) ICP standard solution (Techlab n°B3015042): $2\sigma = 0.08‰$ (n = 137); and b) Henderson molybdenite 8599: $2\sigma = 0.08‰$ (n = 85).

On Fig. 4 we plotted also the mean values and standard deviations for the occurrence types. Even if small differences can be seen in the mean values, it is not possible to differentiate the occurrence/deposit types of molybdenite based on their $\delta^{98}Mo_{NIST}$ values when considering the standard deviation of data (expressed as two standard deviations of the mean value).

Granite and porphyry deposits show lower $\delta^{98}Mo_{NIST}$ mean values (−0.15 and −0.17‰) than the other deposit types, while greisen (1.00‰, n = 3) and IOCG (0.82‰, n = 5) deposits show the highest mean values. Higher crystallization temperature of the former and lower of the latter group could explain these trends/variations. The reasons for Mo-isotope fractionation in molybdenite during magmatic and hydrothermal processes, however, are not well understood at present. Hannah et al. (2007) plead in favour of vapour transport and local Rayleigh distillation of Mo during molybdenite crystallization to explain the Mo isotope values in molybdenites. Although their arguments do not explain all measured values, Hannah et al. (2007) conclude that the "*average isotopic composition of molybdenite from any one occurrence reflects that of continental crust*." Even if the reasons explaining Mo-isotope fractionation in molybdenites remain relatively unknown, isotopic fractionation of Mo can be the result of several processes as recently discussed (Greber et al., 2014; Shafiei et al., 2014). Shafiei et al. (2014) recently evidenced that temperature is a parameter that can influence the partition of the fluid between liquid, vapour and saline brine. Another process leading to the fractionation of Mo isotopes concerns the structural polytype of molybdenite (Shafiei et al., 2014). Greber et al. (2014) discuss the preferential incorporation of Mo isotopes during fractional crystallization of minerals, the heavy Mo isotopes being preferentially incorporated into aqueous hydrothermal fluid, and the light Mo isotopes being incorporated into molybdenite crystals.

The large number of $\delta^{98}Mo_{NIST}$ data in our database (n = 391) permits to run solid statistical analysis. The data distribution resembles the normal distribution (Fig. 5). Arithmetic mean and median, following the definition given in Meibom and Anderson (2003), are close each to other ($0.04 \pm 1.04‰/2\sigma$/and −0.04‰, respectively), giving a good view of the distribution symmetry. The skewness of the data set is close to

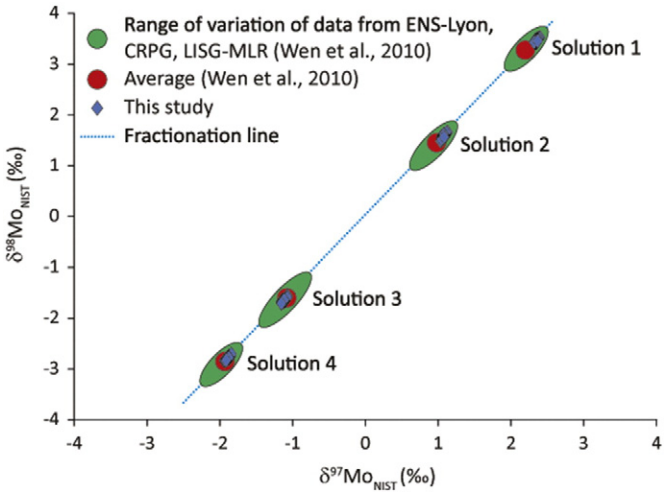

Fig. 3. Plot of $\delta^{97}Mo_{NIST}$ versus $\delta^{98}Mo_{NIST}$ values $_{NIST}$ of four fractionated solutions, and comparison with the results obtained at ENS-Lyon, CRPG Nancy and LISG-MLR (Wen et al., 2010). All data are plotted on the theoretical mass-fractionation line.

Table 2
Mo-isotope data of molybdenites analysed for this study. Data are relative to NIST3134 ($\delta^{98}Mo = 0$). Long-term external reproducibility of 0.08‰ (2σ) on $\delta^{98}Mo$.

Occurrence type	ID	Location	n	$\delta^{97}Mo_{NIST}$	2σ	$\delta^{98}Mo_{NIST}$	2σ
Granite	Mo001	Kigom, Nigeria	6	−0.22	0.04	−0.32	0.06
	Mo031	Becon les granits, Maine-et-Loire, France	5	−0.28	0.08	−0.4	0.06
	Mo032	Becon les granits, Maine-et-Loire, −France	10	−0.48	0.06	−0.71	0.07
	Mo033	Becon les granits, Maine-et-Loire, France	8	−0.23	0.04	−0.34	0.05
	Mo034	Becon les granits, Maine-et-Loire, France	8	−0.01	0.04	−0.02	0.05
	Mo053	Becon les granits, Maine-et-Loire, France	5	−0.3	0.03	−0.48	0.1
	Mo039	Man Departement, Ivory Coast	8	−0.19	0.04	−0.26	0.09
	Mo046	Bamiyan valley, Afghanistan	5	0.38	0.06	0.55	0.09
	Mo047	Traouiéros, Côtes d'Armor, France	5	−0.44	0.04	−0.68	0.08
	Mo167	Wurinitu, Inner Mongolia, China	4	−0.19	0.06	−0.29	0.06
	Mo168	Wurinitu, Inner Mongolia, China	4	−0.19	0.03	−0.31	0.07
	Mo169	Wurinitu, Inner Mongolia, China	4	−0.21	0.07	−0.32	0.08
	Mo170	Wurinitu, Inner Mongolia, China	5	−0.08	0.03	−0.11	0.05
	Mo171	Wurinitu, Inner Mongolia, China	5	−0.19	0.07	−0.28	0.07
Pegmatite	Mo002	Thornborough Hodgkinson Gold Field, Queensland, Australia	6	−0.08	0.06	−0.13	0.12
	Mo009a	Preissac, Abitibi, Canada	6	−0.16	0.05	−0.24	0.07
	Mo009b	Preissac, Abitibi, Canada	5	−0.41	0.03	−0.61	0.06
	Mo010	Château-Lambert, Vosges, France	9	0.77	0.08	1.14	0.12
	Mo012	La clarté Ploumanac'h, Côtes d'Armor, France	5	−0.31	0.06	−0.46	0.08
	Mo026	La clarté Ploumanac'h, Côtes d'Armor, France	8	−0.39	0.08	−0.58	0.12
	Mo061	La clarté Ploumanac'h, Côtes d'Armor, France	9	−0.42	0.05	−0.61	0.09
	Mo062	La clarté Ploumanac'h, Côtes d'Armor, France	9	−0.35	0.1	−0.52	0.15
	Mo064	La clarté Ploumanac'h, Côtes d'Armor, France	5	−0.43	0.06	−0.68	0.12
	Mo065	La clarté Ploumanac'h, Côtes d'Armor, France	5	−0.31	0.05	−0.48	0.06
	Mo066	La clarté Ploumanac'h, Côtes d'Armor, France	5	−0.39	0.08	−0.61	0.09
	Mo067	La clarté Ploumanac'h, Côtes d'Armor, France	5	−0.32	0.06	−0.54	0.12
	Mo045	Nunavik, Québec, Canada	5	−0.14	0.06	−0.23	0.13
	Mo048	Menez Goaillou, France	10	−0.04	0.07	−0.04	0.09
	Mo049	Läven, Norway	6	−0.42	0.05	−0.6	0.09
	Mo050	Ivigtut, Arsuk, Greenland	6	0.45	0.07	0.7	0.11
	Mo051	Ivigtut, Arsuk, Greenland	6	0.39	0.04	0.6	0.1
	Mo052	Ivigtut, Arsuk, Greenland	5	0.16	0.07	0.26	0.09
	Mo069	Cubos e Chao do Castanheiro, Mangualde, Portugal	7	0.34	0.06	0.51	0.13
	Mo094	Sunderbyn, Luleå area, Sweden	6	0.54	0.04	0.8	0.06
	Mo095	Sunderbyn, Luleå area, Sweden	5	−0.11	0.02	−0.15	0.04
	Mo096	Sunderbyn, Luleå area, Sweden	10	0.27	0.07	0.41	0.08
	Mo097	Sunderbyn, Luleå area, Sweden	4	0.57	0.03	0.85	0.05
	Mo120a	Moly Hill mine, La Motte, Abitibi, Canada	4	−0.2	0.02	−0.3	0.04
	Mo120b	Moly Hill mine, La Motte, Abitibi, Canada	4	−0.32	0.04	−0.47	0.06
	Mo120c	Moly Hill mine, La Motte, Abitibi, Canada	4	−0.11	0.03	−0.17	0.02
	Mo121a	Moly Hill mine, La Motte, Abitibi, Canada	4	−0.32	0.06	−0.46	0.05
	Mo121b	Moly Hill mine, La Motte, Abitibi, Canada	4	−0.16	0.03	−0.25	0.04
	Mo121c	Moly Hill mine, La Motte, Abitibi, Canada	4	−0.32	0.05	−0.47	0.06
Perigranitic veins	Mo025	Toul-Porz, Côtes du Nord, France	4	0.74	0.07	1.09	0.09
	Mo028	Montbelleux-Luitré, Ile-et-Vilaine, France	5	0.01	0.07	0.02	0.12
	Mo029	Villeray Parcé, Ille-et-Villaine, France	5	0.02	0.07	0.01	0.11
	Mo030	La Rousselière, Loire-Atlantique, France	13	0.42	0.09	0.62	0.13
	Mo043	Tighza-Djebel Aouam, Morocco	5	0.57	0.03	0.79	0.04
	Mo070	Salto do Lobo, Carris-Gerês, Portugal	9	0.41	0.08	0.62	0.11
Greisen	Mo027	Menez Gouaillou, Coray, Finistère, France	5	−0.22	0.11	−0.35	0.11
	Mo042	Altenberg, Germany	5	0.74	0.07	1.07	0.09
Mo-Porphyry deposit	Mo-Hend	Henderson mine, Colorado, USA	47	−0.13	0.06	−0.19	0.09
	Mo-Hend-b	Henderson mine, Colorado, USA	6	−0.15	0.06	−0.22	0.1
	Mo011	Henderson mine, Colorado, USA	5	−0.4	0.04	−0.6	0.06
	Mo081	Climax, Colorado, USA	9	−0.35	0.07	−0.52	0.11
	Mo082	Climax, Colorado, USA	8	−0.1	0.07	−0.14	0.09
Cu-Porphyry deposit	Mo054	Tilly, Québec, Canada	8	−0.58	0.09	−0.86	0.13
	Mo055	Tilly, Québec, Canada	5	−0.2	0.08	−0.28	0.1
	Mo056	Questa, New Mexico, USA	8	−0.29	0.09	−0.43	0.12
	Mo057	Questa, New Mexico, USA	10	−0.19	0.08	−0.27	0.1
	Mo079	Questa, New Mexico, USA	7	−0.39	0.05	−0.57	0.09
	Mo080	Questa, New Mexico, USA	8	−0.38	0.09	−0.56	0.12
	Mo058	Don-Rouyn, Abitibi, Canada	6	0.15	0.05	0.21	0.11
	Mo059	Don-Rouyn, Abitibi, Canada	6	0.08	0.07	0.12	0.07
	Mo063	Bingham Canyon, Utah, USA	8	−0.39	0.11	−0.58	0.13
	Mo071	Chuquicamata, Chile	7	−0.11	0.06	−0.15	0.12
	Mo098	Tsagaan Suvarga, Omnogovi Province, Mongolia	4	−0.43	0.04	−0.63	0.03
	Mo099	Tsagaan Suvarga, Omnogovi Province, Mongolia	4	−0.59	0.06	−0.86	0.06
	Mo100	Hashitu, China	5	0.13	0.05	0.2	0.09
	Mo101	Hashitu, China	4	0.17	0.08	0.26	0.13
	Mo102	Hashitu, China	4	0.19	0.03	0.27	0.02
	Mo103	Hashitu, China	4	0.17	0.07	0.25	0.07
	Mo104	Hashitu, China	4	0	0.06	0	0.06
	Mo105	Hashitu, China	4	0.16	0.04	0.24	0.04
	Mo106	Hashitu, China	3	0.12	0.06	0.18	0.11

Table 2 (*continued*)

Occurrence type	ID	Location	n	$\delta^{97}Mo_{NIST}$	2σ	$\delta^{98}Mo_{NIST}$	2σ
	Mo107	Hashitu, China	3	0.26	0.05	0.37	0.03
	Mo108	Hashitu, China	4	0.07	0.07	0.1	0.11
	Mo109	Thompson Creek, Idaho, USA	4	−0.11	0.05	−0.18	0.07
	Mo110	Thompson Creek, Idaho, USA	4	−0.12	0.08	−0.16	0.11
	Mo111	Butte, Montana, USA	4	−0.31	0.03	−0.44	0.05
	Mo112	Butte, Montana, USA	4	−0.23	0.04	−0.33	0.05
	Mo113	Butte, Montana, USA	4	0.01	0.02	0.01	0.04
	Mo114	Butte, Montana, USA	6	−0.3	0.06	−0.44	0.1
	Mo115	Butte, Montana, USA	4	0.03	0.08	0.04	0.06
	Mo116	Butte, Montana, USA	4	−0.25	0.04	−0.38	0.09
	Mo117	Butte, Montana, USA	6	−0.27	0.04	−0.4	0.06
	Mo118	Butte, Montana, USA	4	−0.24	0.03	−0.36	0.07
	Mo119	Butte, Montana, USA	3	−0.37	0.06	−0.54	0.09
	Mo122	Sora, Russia	4	−0.37	0.07	−0.55	0.09
	Mo123	Sora, Russia	4	−0.34	0.02	−0.51	0.07
	Mo124	Sora, Russia	4	−0.35	0.06	−0.52	0.08
	Mo125	Sora, Russia	4	−0.42	0.01	−0.6	0.02
	Mo126	Zhireken, Eastern Transbaikalia, Russia	4	−0.18	0.07	−0.26	0.12
	Mo127	Zhireken, Eastern Transbaikalia, Russia	4	−0.28	0.07	−0.41	0.08
	Mo128	Zhireken, Eastern Transbaikalia, Russia	4	−0.12	0.09	−0.16	0.13
	Mo129	Zhireken, Eastern Transbaikalia, Russia	4	−0.15	0.02	−0.21	0.05
	Mo130	Zhireken, Eastern Transbaikalia, Russia	4	−0.15	0.04	−0.25	0.08
	Mo131	Zhireken, Eastern Transbaikalia, Russia	4	−0.05	0.06	−0.09	0.05
	Mo132	Zhireken, Eastern Transbaikalia, Russia	4	−0.25	0.04	−0.36	0.06
	Mo133	Aksug, Russia	4	−0.28	0.03	−0.41	0.03
	Mo134	Aksug, Russia	6	−0.09	0.07	−0.13	0.13
	Mo135	Shaktama, Eastern Transbaikalia, Russia	4	−0.35	0.04	−0.52	0.07
	Mo136	Shaktama, Eastern Transbaikalia, Russia	4	−0.26	0.04	−0.39	0.05
	Mo137	Shaktama, Eastern Transbaikalia, Russia	4	−0.38	0.05	−0.57	0.08
	Mo138	Erdenetuin Ovoo, Mongolia	4	−0.39	0.04	−0.58	0.02
	Mo139	Erdenetiin Ovoo, Mongolia	4	−0.26	0.06	−0.39	0.11
	Mo140	Erdenetiin Ovoo, Mongolia	4	−0.33	0.06	−0.49	0.15
	Mo141	Bugdaya, Eastern Transbaikalia, Russia	4	−0.13	0.06	−0.19	0.07
	Mo149	Bugdaya, Eastern Transbaikalia, Russia	4	0.06	0.07	0.08	0.11
	Mo150	Bugdaya, Eastern Transbaikalia, Russia	4	−0.3	0.09	−0.46	0.07
	Mo151	Bugdaya, Eastern Transbaikalia, Russia	4	−0.07	0.03	−0.12	0.05
	Mo152	Bugdaya, Eastern Transbaikalia, Russia	4	−0.65	0.04	−0.97	0.09
	Mo153	Bugdaya, Eastern Transbaikalia, Russia	4	0.25	0.07	0.36	0.07
	Mo142	Davenda, Eastern Transbaikalia, Russia	4	−0.23	0.02	−0.33	0.07
	Mo143	Davenda, Eastern Transbaikalia, Russia	4	0.22	0.04	0.33	0.05
	Mo144	Davenda, Eastern Transbaikalia, Russia	4	−0.05	0.07	−0.09	0.1
	Mo145	Chubachi, Russia	4	−0.57	0.02	−0.85	0.05
	Mo146	Veseloye, Russia	4	−0.38	0.04	−0.56	0.03
	Mo147	Okonon, Russia	4	−0.27	0.06	−0.42	0.04
	Mo148	Vykhodnoye, Russia	4	0.03	0.04	0.04	0.07
	Mo154	Dasuji-Zhuozi county, Inner Mongolia, China	4	0.14	0.07	0.21	0.12
	Mo155	Caosiyao-Xinghe county, Inner Mongolia, China	4	−0.11	0.02	−0.16	0.04
	Mo156	Caosiyao-Xinghe county, Inner Mongolia, China	4	−0.1	0.06	−0.14	0.08
	Mo157	Caosiyao-Xinghe county, Inner Mongolia, China	4	−0.08	0.08	−0.11	0.1
	Mo158	Caosiyao-Xinghe county, Inner Mongolia, China	4	−0.09	0.08	−0.13	0.07
	Mo159	Caosiyao-Xinghe county, Inner Mongolia, China	4	−0.11	0.06	−0.17	0.1
	Mo160	Caosiyao-Xinghe county, Inner Mongolia, China	4	−0.51	0.02	−0.76	0.03
	Mo161	Caosiyao-Xinghe county, Inner Mongolia, China	4	−0.47	0.03	−0.7	0.06
	Mo162	Ulandler-Sunid Zuoqi area, Inner Mongolia, China	4	−0.04	0.07	−0.07	0.1
	Mo163	Ulandler-Sunid Zuoqi area, Inner Mongolia, China	4	−0.05	0.05	−0.07	0.06
	Mo164	Ulandler-Sunid Zuoqi area, Inner Mongolia, China	4	−0.04	0.02	−0.07	0.06
	Mo165	Ulandler-Sunid Zuoqi area, Inner Mongolia, China	4	−0.06	0.02	−0.09	0.01
	Mo166	Ulandler-Sunid Zuoqi area, Inner Mongolia, China	4	−0.03	0.02	−0.04	0.03
	Mo172	Donggebi, Tianshan, China	5	0.09	0.06	0.14	0.07
	Mo173	Dongchuan, Yunnan, China	5	0.57	0.02	0.84	0.05
	Mo174	Linxi, Inner Mongolia, China	5	−0.19	0.02	−0.28	0.01
	Mo175	Linxi, Inner Mongolia, China	5	−0.13	0.03	−0.19	0.04
	Mo176	Donggebi, Tianshan, China	5	−0.32	0.05	−0.47	0.09
	Mo177	Donggebi, Tianshan, China	5	−0.21	0.02	−0.32	0.05
	Mo178	Donggebi, Tianshan, China	5	0.18	0.03	0.27	0.04
	Mo179	Donggebi, Tianshan, China	5	−0.4	0.03	−0.59	0.07
Skarn	Mo004	Azegour, Morocco	6	0.05	0.09	0.07	0.11
	Mo007	Azegour, Morocco	6	−0.29	0.08	−0.43	0.09
	Mo008	Azegour, Morocco	6	0.21	0.05	0.32	0.09
	Mo072	Azegour, Morocco	5	−0.35	0.06	−0.55	0.1
	Mo073	Azegour, Morocco	6	−0.4	0.09	−0.6	0.12
	Mo074a	Azegour, Morocco	5	0.21	0.07	0.25	0.12
	Mo074b	Azegour, Morocco	5	−0.08	0.03	−0.17	0.09
	Mo074c	Azegour, Morocco	6	−0.02	0.05	−0.08	0.06
	Mo075a	Azegour, Morocco	6	0.13	0.09	0.16	0.2

(*continued on next page*)

Table 2 (*continued*)

Occurrence type	ID	Location	n	$\delta^{97}Mo_{NIST}$	2σ	$\delta^{98}Mo_{NIST}$	2σ
Skarn	Mo075b	Azegour, Morocco	6	0.23	0.07	0.29	0.1
	Mo076a	Azegour, Morocco	6	−0.08	0.07	−0.17	0.11
	Mo076b	Azegour, Morocco	6	0.32	0.07	0.42	0.13
	Mo077	Azegour, Morocco	6	0.3	0.07	0.4	0.13
	Mo078	Azegour, Morocco	6	0.08	0.1	0.08	0.19
	Mo084a	Azegour, Morocco	5	−0.18	0.04	−0.26	0.08
	Mo084b	Azegour, Morocco	5	−0.09	0.02	−0.14	0.05
	Mo084c	Azegour, Morocco	5	−0.2	0.02	−0.31	0.02
	Mo085a	Azegour, Morocco	5	−0.09	0.09	−0.13	0.1
	Mo085b	Azegour, Morocco	5	0.02	0.08	0.04	0.08
	Mo085c	Azegour, Morocco	5	−0.14	0.04	−0.17	0.05
	Mo085d	Azegour, Morocco	5	−0.08	0.03	−0.1	0.04
	Mo086a	Azegour, Morocco	8	−0.13	0.09	−0.19	0.14
	Mo086b	Azegour, Morocco	5	−0.18	0.07	−0.27	0.12
	Mo087	Azegour, Morocco	5	0.18	0.06	0.26	0.11
	Mo088a	Azegour, Morocco	5	0.03	0.05	0.04	0.04
	Mo088b	Azegour, Morocco	5	0.17	0.07	0.25	0.1
	Mo089a	Azegour, Morocco	5	0.03	0.07	0.04	0.1
	Mo089b	Azegour, Morocco	5	0.27	0.04	0.41	0.06
	Mo090	Azegour, Morocco	5	0.11	0.04	0.18	0.08
	Mo035	Dielette-Flamanville, Manche, France	5	0	0.08	0.01	0.13
	Mo036	Dielette-Flamanville, Manche, France	10	−0.08	0.1	−0.11	0.13
	Mo040	Isk Imoula, Tichka, Morocco	8	0.09	0.04	0.14	0.07
	Mo041	Ikissane, Tichka, Morocco	6	0.51	0.08	0.75	0.12
	Mo083	Edwards, New York, USA	6	0.1	0.07	0.15	0.1
Alpine-type fissure veins	Mo013	La Meije, Hautes Alpes, France	6	0.31	0.06	0.45	0.07
	Mo014	Combe Laurichard, Hautes Alpes, France	5	0.06	0.09	0.08	0.07
	Mo015	Glacier de l'homme,Hautes Alpes, France	5	0.89	0.09	1.31	0.11
	Mo016	Clos l'Oureou, Hautes Alpes, France	6	−0.05	0.07	−0.06	0.08
	Mo017	Clos l'Oureou, Hautes Alpes, France	6	−0.07	0.06	−0.1	0.06
	Mo018	Glacier de Bonne Pierre, Isère, France	5	−0.03	0.06	−0.04	0.11
	Mo019	Glacier de Bonne Pierre, Isère, France	6	0.54	0.02	0.79	0.04
	Mo020	Glacier de Bonne Pierre, Isère, France	5	−0.31	0.09	−0.45	0.08
	Mo021	Ravin de la Ruine, Isère, France	5	−0.08	0.06	−0.11	0.06
	Mo022	Ravin de la Ruine, Isère, France	8	0.27	0.07	0.39	0.1
	Mo023	Ravin de la Ruine, Isère, France	7	0.77	0.04	1.14	0.03
	Mo024	Tête du Rouget, Isère, France	4	−0.13	0.05	−0.2	0.09
	Mo037	Baltschiedertal, Switzerland	9	0.2	0.09	0.3	0.15
	Mo038	Baltschiedertal, Switzerland	6	0.28	0.05	0.43	0.08
	Mo060	Stilluptal, Zillertal, Austria	6	0.16	0.06	0.26	0.1
IOCG	Mo091	Lala, China	8	0.21	0.08	0.3	0.12
Unknown origin	Mo003	Spain	6	0.33	0.07	0.48	0.1
	Mo005	Morocco	6	−0.05	0.03	−0.08	0.05
	Mo006	Québec, Canada	6	−0.31	0.07	−0.46	0.08
	Mo044	Cameroon	8	0.62	0.07	0.91	0.09
	Mo068	Borralha, Portugal	7	0.09	0.09	0.13	0.15
	Mo092	Sunderbyn, Luleå area, Sweden	10	0.31	0.06	0.47	0.08
	Mo093	Sunderbyn, Luleå area, Sweden	10	0.6	0.05	0.89	0.06

0.62, reflecting a slightly left-derived distribution; if the distribution would be symmetric, then the mean is equal to the median and the distribution will have zero skewness. In the end, the excess kurtosis was also calculated; this is an estimate of the peakedness of the distribution compared to a Gaussian one. The dataset have an excess kurtosis of 1.029, reflecting a distribution that resembles a Gaussian one (with an excess kurtosis of 0). The slightly positive value of the excess kurtosis indicates a moderately peaked distribution. A Gaussian (normal) distribution is often used in pattern-recognition problems as the best way of modelling the probability density of experimental data; it is the distribution of the disorder maximum among all possible distributions coupling a defined mean and variance. Therefore, applying Gaussian distribution to a data set helps avoiding particular cases.

The distribution fits well with a Gaussian curve (pointed line in Fig. 5) with an R^2 close to 0.52. The Kolmogorov–Smirnov non-parametric test — used for testing the normality of the distribution — fits also with the assumption that the $\delta^{98}Mo_{NIST}$ data distribution is Gaussian. Furthermore, the probability-probability plot (P–P plot) on Fig. 6, is a graph of the empirical cumulative-distribution function values plotted against the theoretical ones. This is a step function that jumps up by 1/n at each of the n data points. The P–P plot is used for determining how well a specific distribution fits the observed data. This plot will be approximately linear if the specified theoretical distribution is the correct model. According to Fig. 6, the quasi-linearity of the pattern shows that the measurements are normally distributed. However, irregularities in the peak and potential contribution of the outliers can be tested by calculating a reduced chi-square value. The value for a pure normally distributed data set should be 1. The calculated value is 14 (e.g. $\chi 2$ observed = 391 divided by the number of degrees of freedom $\nu = 27$) that reflects irregularities.

Another insight of this new data set concerns the implications for the global Mo cycle. Voegelin et al. (2014) postulate the difficulties in defining the Mo isotope composition of the upper continental crust. Following other investigations, they used an alternative approach to constrain the Mo-isotope signature of the bulk silicate crust by using molybdenite-isotope values. This assumption is based on the fact that molybdenite is the only mineral source of Mo and originates from crystallizing magma or from hydrothermal processes. Thus, molybdenite provides a robust proxy for a crustal Mo-isotope signature. Following Greber et al. (2011), Voegelin et al. (2014) used the published molybdenite Mo-isotope data and calculated the average value of $\delta^{98}Mo_{NIST} = 0.15‰$ (after normalization to the NIST3134 at 0‰). This value is clearly different from the one we defined in this study (mean value of 0.04‰). Arguing like Voegelin et al. (2014),

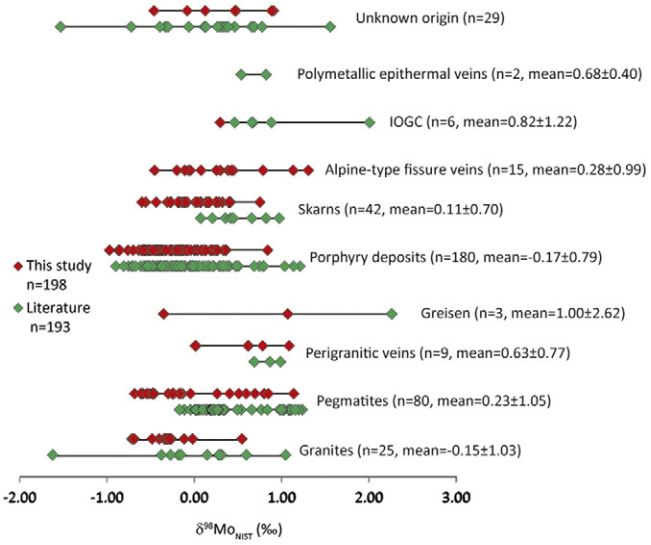

Fig. 4. $\delta^{98}Mo_{NIST}$ variations of molybdenite for the different occurrence/deposit types: granite, pegmatite, perigranitic vein, greisen, porphyry deposit, skarn, Alpine-type fissure vein, IOCG, polymetallic epithermal vein and unknown origin (this study and the literature, see text for details). Number of samples, mean value and 2σ (standard deviation) are given for each occurrence/deposit type.

the wide variation of $\delta^{98}Mo_{NIST}$ over a few per mil precludes the use of molybdenite Mo-isotope ratios for constraining the value of the silicate crust. This is confirmed by the two standard deviations of the whole data set (1.04).

Our database helps investigating the nature of Mo-isotope fractionation, as well as testing any links with mineralizing processes. In order to demonstrate this we will focus on the granite-pegmatite-perigranitic vein series. For these occurrences (Fig. 7), we see that the mean $\delta^{98}Mo_{NIST}$ values evolve from granite ($-0.15‰ \pm 1.03$, $n = 25$) to pegmatite ($0.23‰ \pm 1.05$, $n = 80$) and finally to perigranitic veins ($0.63‰ \pm 0.77$, $n = 9$). The mean greisen value is not significant for this comparison as only three values can be used for the calculation. Measurements of the arithmetic mean and median are close for individual molybdenite occurrences, with, respectively for the mean and the median, −0.16 and −0.27 for granite, 0.23 and 0.20 for pegmatite, and 0.63 and 0.69 for perigranitic veins. For each occurrence, the similarity of the mean and median values indicates a distribution symmetry. This is also documented by the coefficient of variation (CV), ranging from −3.2 for granite, 2.3 for pegmatite and 0.6 for perigranitic veins, measuring the dispersion of samples whose means are not equal. The skewness of the three data subsets are respectively close to −0.22, 0.20 and −0.73 for granite, pegmatite and perigranitic veins. These values reflect a slightly left-derived distribution for the pegmatite and a slightly right-derived distribution for the granite and the perigranitic veins. The $\delta^{98}Mo_{NIST}$ ratios of molybdenites have an excess kurtosis of respectively 2.39, −0.74 and −0.23 for granite, pegmatite and perigranitic veins, reflecting distributions that resemble a Gaussian one (with an excess kurtosis of 0). The positive value for granite indicates a peaked distribution, while the slightly negative values for pegmatite and perigranitic veins indicates a more smoothed distribution.

Lower $\delta^{98}Mo_{NIST}$ values (Figs. 4 and 7) are found in molybdenite-bearing granite, while perigranitic veins have the highest mean values. We used the Kruskal–Wallis analysis for comparing the $\delta^{98}Mo_{NIST}$ values obtained for these Mo occurrences, as the distribution of $\delta^{98}Mo_{NIST}$ values does not meet the normality assumption. Indeed, if each distribution would be symmetric, then the mean might be equal to the median and the distribution will have zero skewness. The results of the Kruskal–Wallis analysis show two features: the p-value is <0.05 when comparing granite-related molybdenite with the rest, and it is >0.05 when comparing molybdenite from pegmatite and perigranitic veins. This suggests that the pegmatite —and perigranitic veins— molybdenite means are statistically equal, but that both differ from the value for granite-molybdenite. The fractionation processes for Mo isotopes could thus be higher when the temperature decreases (Greber et al., 2014).

Granites crystallize at temperatures between 600 and 1000 °C and molybdenites can occur within the granitic intrusion, or in the surrounding rocks. The crystallization temperatures are between 350 °C to 450 °C for the pegmatites (London, 2009). Perigranitic veins form later than pegmatites, at the end of granite crystallizing stage when the crystallization temperature is lower, below the pneumatolytic to hydrothermal transition (about 374 °C). Not only is the crystallization temperature close for molybdenite from pegmatites and perigranitic veins with comparable means, but it is different between granite-related molybdenite and molybdenite from pegmatites. This indicates that the crystallization temperature influences the $\delta^{98}Mo_{NIST}$ values of granite-related occurrences. In addition, we can postulate that these differences, being related to the preferential incorporation of light Mo-isotopes during crystallization, will leave behind a melt enriched in heavier Mo isotopes. Greber et al. (2014) proposed this explanation at the occurrence scale, but with our new data we can extend this explanation to a larger scale.

Hannah et al. (2007) claimed no relationship between $\delta^{98}Mo_{NIST}$ and the age of mineralization. In the new data set we obtained for this study, the samples came from all continents —especially new data from Russia and China— and cover Archean to "Recent" (<2 Ma) times. Again, no relationship was observed between the isotope ratio and the age of mineralization.

4.2. Variability of $\delta^{98}Mo_{NIST}$ at occurrence scale

For some occurrences, we could analyse $\delta^{98}Mo_{NIST}$ values on several molybdenite samples. For the Bécon-les-Granits granite (Maine-et-Loire, France), from where five molybdenite samples were analysed, the $\delta^{98}Mo_{NIST}$ variation is around 0.69‰. Alpine-type fissure veins show even larger variations close to 1.25‰, as observed for both Glacier de Bonne Pierre ($n = 3$) and Ravin de la Ruine ($n = 3$).

Focusing on data subset covering skarns, pegmatites and porphyry deposits, we applied the box-plots approach (Fig. 8). This uses the median, quartiles, and lowest and highest data points for conveying the level, spread, and symmetry of a distribution of data values, and is easily refined to identify outlier data values.

For the Azegour skarn (Morocco, Permingeat, 1959; Breillat et al., 2013), the $\delta^{98}Mo_{NIST}$ values of the 29 molybdenite samples cover a large range of variations, around 0.7‰, from −0.60 to 0.42‰. Compared to the other skarn samples ($n = 42$; Fig. 8a), it is clear that the Azegour group is generally similar, the median being lower than the value for all 42 skarn samples (inclusive the Azegour), the minima being close for the two sample sets while the maxima are higher in the whole skarn population.

Considering the pegmatite occurrences, Fig. 8b shows the Alpajahorn site (Swiss Alps, $n = 38$, Greber et al., 2011), the Grimsel Pass site (Swiss Alps, $n = 13$, Greber et al., 2011), the Ploumanac'h pegmatite from Brittany (NW France; this study, $n = 8$) as well as the whole pegmatite data set ($n = 80$). Taken as a whole, the pegmatite population attains a median value of 0.21‰. The Ploumanac'h pegmatite $\delta^{98}Mo_{NIST}$ varies slightly by only 0.22‰, between the lowest value ($\delta^{98}Mo_{NIST} = -0.68‰$) and the highest one ($\delta^{98}Mo_{NIST} = -0.46‰$), with median $\delta^{98}Mo_{NIST}$ values of around −0.58‰ and a clearly Gaussian data distribution. Compared to the whole data set, the Ploumanac'h pegmatite occupies the lowermost values. For the Alpajahorn site data distribution is clearly non-gaussian, Greber et al. (2011) argued that the most plausible Mo source is related to the circulation of hydrothermal fluids exsolved during late crystallization stages of the Central Aar Massif granite. For the Ploumanac'h pegmatite, the Mo source is similar - late residual magmatic fluids. Moreover, Greber et al. (2011)

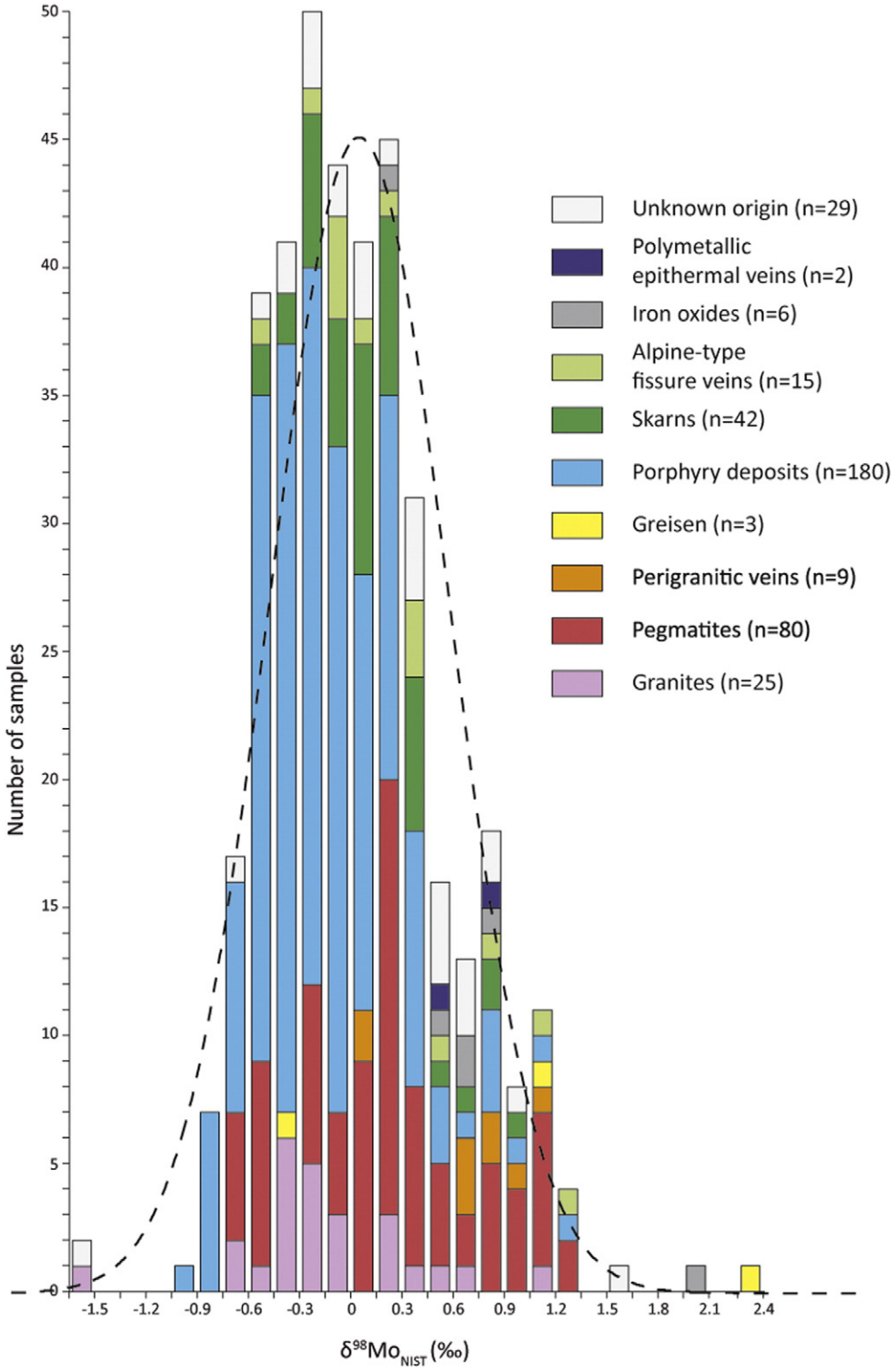

Fig. 5. Histogram of $\delta^{98}Mo_{NIST}$ ratios of molybdenite in the different occurrence types (same list as Fig. 4). The curve (dotted line) indicates the Gaussian distribution that best fits the observed data: mean = 0.04; 2σ (standard deviation) = 1.04.

proposed redox variations of the mineralizing fluids as the main mechanism for explaining the isotopic variations in the Alpajahorn site. For the Ploumanac'h occurrence, the narrow range of data variation may reflect short transport distance of the fluid related to the proximity of the parent granite to the pegmatite-host.

For the porphyry occurrences (n = 180) the distribution is Gaussian. Fig. 8c shows the data for a selected series of sites. These include the Butte deposit (Rusk et al., 2008; USA, n = 9, this study), the Caosiyao deposit (China, n = 7, this study), the Hashitu deposit (Zhai et al., 2014; China, n = 9, this study), the Questa deposit (USA, n = 46, this study and Greber et al., 2014), the Kerman deposit (Iran, n = 26, Shafiei et al., 2014), the Bugdaya deposit (Kovalenker et al., 2011; Russia, n = 6, this study), and the Zhireken deposit (Berzina and Sotnikov, 2010; Russia, n = 7, this study). Statistical parameters for the box plot of the Zhireken, Kerman, Questa and Hashitu deposits show a clearly Gaussian distribution. Bugdaya, Butte and

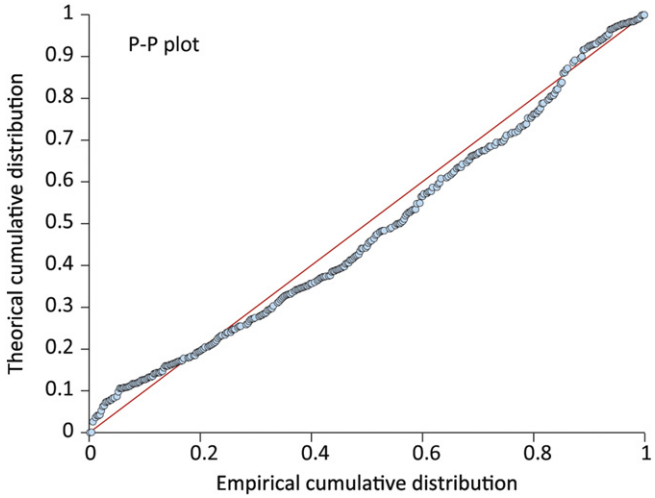

Fig. 6. Probability–Probability (P–P) plot showing the fit with a normal law with a mean value of 0.04‰ and a 2σ of 1.04‰.

Cosiyao are clearly non-Gaussian distribution. Kerman deposit shows the largest variation ($\delta^{98}Mo_{NIST}$ min = −0.90‰; max = 1.04‰; median = −0.03‰) almost identical to the range of the whole porphyry-deposit data set. For Butte deposits, outliers induce a mean value higher than the 75th percentile. However, when comparing all sites —with the exception of Hashitu—, the median values are close to that for porphyry deposits as a whole at −0.22‰.

4.3. Variability of $\delta^{98}Mo_{NIST}$ at sample scale

Variations of the $\delta^{98}Mo_{NIST}$ at centimetre scale were observed by Hannah et al. (2007) and Greber et al. (2011). Several explanations are possible for this variability, including a late metamorphic event (marked by a multi-modality of $\delta^{98}Mo_{NIST}$, Greber et al., 2011); multi-stage crystallization of molybdenite identifiable by Re-Os dating of the molybdenites (Greber et al., 2014) with igneous and hydrothermal molybdenite and molybdenite crystallized in stockworks; and finally by a Rayleigh fractionation that could explain a variation of up to 0.6‰ (Hannah et al., 2007; Greber et al., 2014). We confirmed this by analysing different samples. First, two molybdenite samples from the Preissac pegmatite (Abitibi, Canada) were analysed; within the rock sample they were about 3 cm distant, but their $\delta^{98}Mo_{NIST}$ values differed by 0.36‰, higher than the analytical uncertainty of 0.09‰. After that, we analysed two samples from the Moly Hill pegmatite (La Motte, Abitibi, Canada). In the first one, three molybdenite spots —about 2 cm distant— were analysed, displaying a $\delta^{98}Mo_{NIST}$ variation of around 0.30‰. In the second sample, three molybdenites —again about 2 cm distant— showed a variation of 0.22‰ in the $\delta^{98}Mo_{NIST}$ values. It is clear that more work is needed to investigate the link between

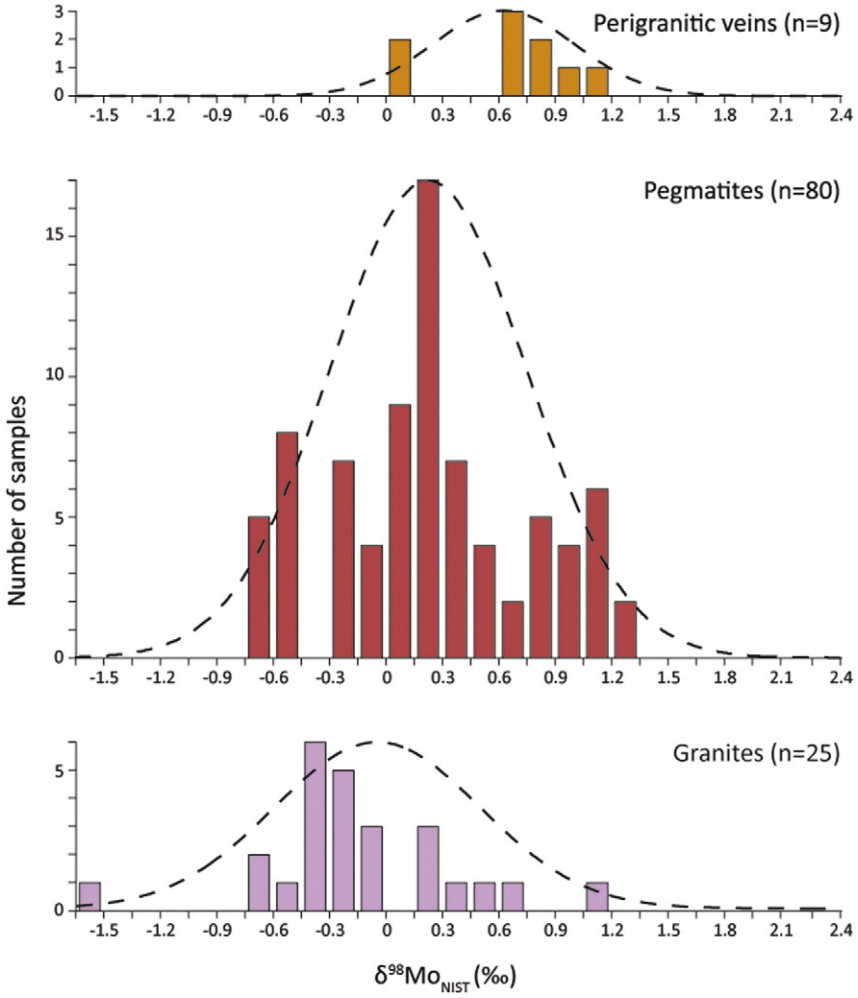

Fig. 7. Histogram of $\delta^{98}Mo_{NIST}$ ratios of MoS_2 in granite, pegmatite and perigranitic vein. The curve (dotted line) indicates the Gaussian distribution for each deposit type that best fits the observed data.

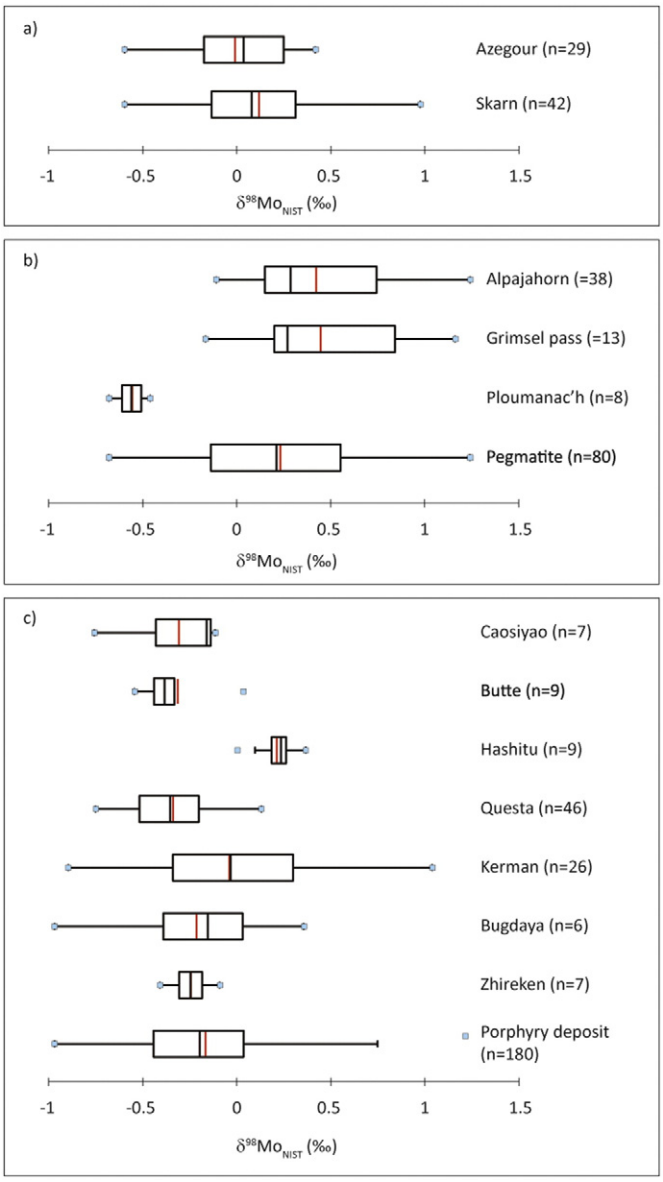

Fig. 8. Box plots of $\delta^{98}Mo_{NIST}$ ratios in molybdenites according to the occurrence types (this study and the literature, see text for details); a) skarn, b) pegmatite and c) porphyry deposit. The red vertical line represents the mean value and the black vertical line the median value; the box represents 1st and 3rd quartiles. The horizontal line corresponds to minimum and maximum accepted values. The symbols mark outliers.

$\delta^{98}Mo_{NIST}$ variations and the main causes of the fractionation processes, a work that was started with the Azegour case (Breillat et al., 2013).

5. Conclusions

We used variations in the Mo-isotopic composition in molybdenites (MoS_2) for studying the different types of ore deposits and particularly for understanding Mo fractionation during mineralizing processes.

A key question when using large data sets (combining data from this study and the literature) concerns the standard problem of normalizing data. As there is no international standard for Mo-isotopes, uncertainties remain when comparing data sets from different laboratories. To solve this potential problem, we used the NIST3134 —proposed as an international standard— to obtain meaningful access to different data deriving from world-wide molybdenite occurrences.

The molybdenite database used in this study thus comprises 391 Mo-isotope data, including 193 samples from the literature and 198 from this work. Thanks to this study, the number of available $\delta^{98}Mo_{NIST}$ data for molybdenite has been more than doubled. The concerned ore-deposits are porphyries, skarns, pegmatites, perigranitic veins, greisen, Alpine-type fissure veins, IOCG, epithermal veins, and a few Mo samples of undetermined origin.

The obtained $\delta^{98}Mo_{NIST}$ values varied greatly from −1.62 to 2.27‰, with the largest range for MoS_2 of greisen and granite (2.6‰). Differences can be seen in the mean values, but we could not differentiate $\delta^{98}Mo_{NIST}$ according to occurrence type when using two standard deviations of the mean value. The crystallization temperature can explain some variations, as perigranitic veins, greisen, Alpine-type fissure veins and polymetallic veins generally crystallize at lower temperatures than granite, pegmatite and porphyry deposits. Although most of studied deposits can form over a wide temperature range, granite, pegmatite, perigranitic veins and porphyry deposits usually show high formation temperatures, near to solidus temperatures of related magmas. Skarns and IOCG are more delicate, as sulphides can be deposited at various stages of the metasomatic process.

The 391 data set yielded a mean value of 0.04 ± 1.04‰ (2σ) and a median value of −0.04‰ $\delta^{98}Mo_{NIST}$, both showing good symmetry in the distribution. This agrees with the data skewness, which reflects a slightly left-derived distribution, and the excess kurtosis that reflects a Gaussian and peaked distribution. The Kolmogorov–Smirnov nonparametric test for testing the distribution normality, confirmed the assumption that the distribution of all data is Gaussian.

A Kruskal–Wallis analysis of the $\delta^{98}Mo_{NIST}$ molybdenite distribution of the granite-pegmatite-perigranitic veins data subsets confirmed that the mean values of pegmatite and perigranitic veins are statistically (test of the mean) undistinguishable, however, are different from that of granites. As proposed by Greber et al. (2014), we explain these differences by a preferential incorporation of light Mo isotopes into molybdenite during crystallization from an aqueous fluid, leaving a melt enriched in heavier Mo isotopes. In a granitic-perigranitic environment, a trend of average values can be drawn from highest to lowest temperatures: granite (−0.13‰), pegmatite (0.23‰), perigranitic veins (0.63‰) and greisen (1.00‰). Other processes could explain these variations as Rayleigh fractionation (Hannah et al., 2007) and the structural type of molybdenites in the crystal structure (Shafiei et al., 2014).

It is important to work with the same standard for improving data reproducibility, and in order to have a better understanding of Mo-isotopic-composition variations at smaller scales. Thanks to the NIST3134 normalization, a huge data set could be compared. The large number of samples analysed for this study allowed refining the Mo-isotopic composition database, as the variations are smaller in our data set than in the literature data sets.

Supplementary data to this article can be found online at http://dx.doi.org/10.1016/j.gexplo.2015.07.019.

Acknowledgments

This work is part of the first author's PhD research supported by the Region Centre (Grant number: 201100069392) and the Carnot-BRGM Institute (Action 2011-02). We thank Anne-Marie Desaulty, Anne-Marie Gallas and Michèle Robert for their help during laboratory work. Wen et al. are thanked for providing us with fractionated solutions. We acknowledge our BRGM colleagues Delphine Bruyère, Thierry Augé, Laurent Bailly, Wolfram Kloppmann and Johan Tuduri in helping us to find samples in the BRGM collection. Several colleagues from other institutes provided us with molybdenite samples or advice: Daniel P.S. de Oliveira (LNEG, Portugal), Richard Wanty (US Geological Survey, USA), Jeffrey Chiarerzelli (St. Lawrence University, USA), Michel Jébrak and Emilie Delpech (UQAM, Canada), Hans Isaksson (Geovista Luleå, Sweden), Degao Zhai (State Key Laboratory of Geological Processes and

Mineral Resources, China, University of Geosciences, Beijing, China, Department of Geological Sciences, Indiana University, Bloomington, Indiana, USA), Anita Berzina (Institute of Geology and Mineralogy, Novosibirsk, Russia), Vladimir Kovalenker (Institute of Geology of Ore Deposits, Petrography, Mineralogy, and Geochemistry, Russian Academy of Sciences, Moscow, Russia), and Jianjun Liu (China University of Geosciences, Beijing, China). We are grateful to Dr. H.M. Kluijver for proofreading and editing the English text. A special thank goes to the anonymous reviewer, Ryan Mathur and the Associate Editor for constructive criticism.

References

Anbar, A.D., 2004. Molybdenum stable isotopes: observations, interpretations and directions. Rev. Mineral. Geochem. 55, 429–454.

Anbar, A.D., Knab, K.A., Barling, J., 2001. Precise determination of mass-dependent variations in the isotopic composition of molybdenum using MC-ICP-MS. Anal. Chem. 73, 1425–1431. http://dx.doi.org/10.1021/ac000829w.

Archer, C., Vance, D., 2008. The isotopic signature of the global riverine molybdenum flux and anoxia in the ancient oceans. Nat. Geosci. 1, 597–600. http://dx.doi.org/10.1038/ngeo282.

Arnold, G.L., Anbar, A.D., Barling, J., Lyons, T.W., 2004. Molybdenum isotope evidence for widespread anoxia in mid-proterozoic oceans. Science 304, 87–90. http://dx.doi.org/10.1126/science.1091785.

Ballard, J.R., Palin, J.M., Williams, I.S., Campbell, I.H., Faunes, A., 2001. Two ages of porphyry intrusion resolved for the super-giant Chuquicamata copper deposit of northern Chile by ELA-ICP-MS and SHRIMP. Geology 29, 383–386. http://dx.doi.org/10.1130/0091-7613(2001)029<0383:TAOPIR>2.0.CO;2.

Barling, J., Arnold, G.L., Anbar, A.D., 2001. Natural mass-dependent variations in the isotopic composition of molybdenum. Earth Planet. Sci. Lett. 193, 447–457.

Berzina, A., Sotnikov, V.I., 2010. Contribution from mafic melt to the Zhireken porphyry Mo–Cu deposit, eastern Transbaikalia, Russia: evidence from mafic microgranular enclaves. Int. J. Econ. Environ. Geol. 1, 42–45.

Borrok, D.M., Nimick, D.A., Wanty, R.B., Ridley, W.I., 2008. Isotopic variations of dissolved copper and zinc in stream waters affected by historical mining. Geochim. Cosmochim. Acta 72, 329–344. http://dx.doi.org/10.1016/j.gca.2007.11.014.

Breillat, N., Guerrot, C., Négrel, P., Marcoux, E., 2013. $\delta^{97/95}$Mo in molybdenites from the Azegour skarn (Morocco). Goldschmidt conference, August 25–30, Florence, Italy. Mineral. Mag. 77, 767.

Chappaz, A., Lyons, T.W., Gordon, G.W., Anbar, A.D., 2012. Isotopic fingerprints of anthropogenic molybdenum in lake sediments. Environ. Sci. Technol. 46, 10934–10943. http://dx.doi.org/10.1021/es3019379.

Chen, H., 2008. The Marcona — Mina Justa district, south-central Peru: implications for the genesis and definition of the iron oxide-copper (-gold) ore deposit clan (PhD thesis, 280 pp.).

Geraghty, E.P., Carten, R.B., Walker, B.M., 1988. Tilting of Urad-Henderson and climax porphyry molybdenum systems, central Colorado, as related to northern Rio Grande rift tectonics. Geol. Soc. Am. Bull. 11, 1780–1786. http://dx.doi.org/10.1130/0016-7606(1988)100<1780:TOUHAC>2.3.CO;2.

Goldberg, T., Gordon, G., Izon, G., Archer, C., Pearce, C.R., McManus, J., Anbar, A.D., Rehkämper, M., 2013. Resolution of inter-laboratory discrepancies in Mo isotope data: an intercalibration. J. Anal. At. Spectrom. 28, 724–735. http://dx.doi.org/10.1039/C3JA30375F.

Greber, N.D., Hofmann, B.A., Voegelin, A.R., Villa, I.M., Nägler, T.F., 2011. Mo isotope composition in Mo-rich high- and low-T hydrothermal systems from the Swiss Alps. Geochim. Cosmochim. Acta 75, 6600–6609. http://dx.doi.org/10.1016/j.gca.2011.08.034.

Greber, N.D., Siebert, C., Nägler, T.F., Pettke, T., 2012. $\delta^{98/95}$Mo values and molybdenum concentration data for NIST SRM 610, 612 and 3134: towards a common protocol for reporting Mo data. Geostand. Geoanalytical Res. 36-3, 291–300. http://dx.doi.org/10.1111/j.1751-908X.2012.00160.x.

Greber, N.D., Pettke, T., Nägler, T.F., 2014. Magmatic–hydrothermal molybdenum isotope fractionation and its relevance to the igneous crustal signature. Lithos 190-191, 104–110. http://dx.doi.org/10.1016/j.lithos.2013.11.006.

Hannah, J.L., Stein, H.J., Wieser, M.E., de Laeter, J.R., Varner, M.D., 2007. Molybdenum isotope variations in molybdenite: vapor transport and rayleigh fractionation of Mo. Geology 35, 703–706. http://dx.doi.org/10.1130/G23538A.1.

Kovalenker, V.A., Kiseleva, G.D., Krylova, T.L., Andreeva, O.V., 2011. Mineralogy and ore formation conditions of the Bugdaya Au-bearing W–Mo porphyry deposit, eastern Transbaikal region, Russia. Geol. Ore Depos. 53, 93–125. http://dx.doi.org/10.1134/S1075701511020048.

Lane, S., Proemse, B.C., Tennant, A., Wieser, M.E., 2013. Concentration measurements and isotopic composition of airborne molybdenum collected in an urban environment. Anal. Bioanal. Chem. 405, 2957–2963. http://dx.doi.org/10.1007/s00216-012-6660-9.

Lee, D.C., Halliday, A.N., 1995. Precise determinations of the isotopic compositions and atomic weights of molybdenum, tellurium, tin and tungsten using ICP magnetic sector multiple collector mass spectrometry. Int. J. Mass Spectrom. Ion Process. 146 (147), 35–46. http://dx.doi.org/10.1016/0168-1176(95)04201-U.

London, D., 2009. Pegmatites. Can. Mineral. Spec. Publ. 10, 363.

Malinovsky, D., Rodushkin, I., Baxter, D.C., Ingri, J., Öhlander, B., 2005. Molybdenum isotope ratio measurements on geological samples by MC-ICPMS. Int. J. Mass Spectrom. 245, 94–107. http://dx.doi.org/10.1016/j.ijms.2005.07.007.

Malinovsky, D., Hammarlund, D., Ilyashuk, B., Martinsson, O., Gelting, J., 2007. Variations in the isotopic composition of molybdenum in freshwater lake systems. Chem. Geol. 236, 181–198. http://dx.doi.org/10.1016/j.chemgeo.2006.09.006.

Markey, R., Stein, H.J., Hannah, J.L., Zimmerman, A., Selby, D., Creaser, R.A., 2007. Standardizing Re–Os geochronology: a new molybdenite reference material (Henderson, USA) and the stoichiometry of Os salts. Chem. Geol. 244, 74–87. http://dx.doi.org/10.1016/j.chemgeo.2007.06.002.

Markl, G., Lahaye, Y., Schwinn, G., 2006. Copper isotopes as monitors of redox processes in hydrothermal mineralization. Geochim. Cosmochim. Acta 70, 4215–4228. http://dx.doi.org/10.1016/j.gca.2006.06.1369.

Mathur, R., Brantley, S., Anbar, A., Munizaga, F., Maksaev, V., Newberry, R., Vervoort, J., Hart, G., 2010. Variation of Mo isotopes from molybdenite in high-temperature hydrothermal ore deposits. Mineral. Deposita 45, 43–50. http://dx.doi.org/10.1007/s00126-009-0257-z.

Mathur, R., Munk, L., Nguyen, M., Gregory, M., Annell, H., Lang, J., 2013. Modern and paleofluid pathways revealed by Cu isotope compositions in surface waters and ores of the pebble porphyry Cu-Au-Mo deposit, Alaska. Econ. Geol. 108, 529–541. http://dx.doi.org/10.2113/econgeo.108.3.529.Mathur et al. 2013.

Meibom, A., Anderson, D.L., 2003. The statistical upper mantle assemblage. Earth Planet. Sci. Lett. 217, 123–139. http://dx.doi.org/10.1016/S0012-821X(03)00573-9.

Murthy, V.R., 1963. Elemental and isotopic abundances of molybdenum in some meteorites. Geochim. Cosmochim. Acta 27, 1171–1178. http://dx.doi.org/10.1016/0016-7037(63)90098-X.

Nägler, T.F., Anbar, A.D., Archer, C., Goldberg, T., Gordon, G.W., Greber, N.D., Siebert, C., Sohrin, Y., Vance, D., 2013. Proposal for an international molybdenum isotope measurement standard and data representation. Geostand. Geoanalytical Res. 38, 149–151. http://dx.doi.org/10.1111/j.1751-908X.2013.00275.x.

Neubert, N., Heri, A.R., Voegelin, A.R., Nägler, T.F., Schlunegger, F., Villa, I.M., 2011. The molybdenum isotopic composition in river water: constraints from small catchments. Earth Planet. Sci. Lett. 304, 180–190. http://dx.doi.org/10.1016/j.epsl.2011.02.001.

Permingeat, F., 1959. Le gisement de molybdène, tungsten et cuivre d'Azegour (Haut Atlas) : etude pétrographique et métallogénique. Notes et Mémoires SGM 141 (PhD thesis, 290 pp.).

Pietruszka, A.J., Walker, R.J., Candela, P.A., 2006. Determination of mass-dependent molybdenum isotopic variations by MC-ICP-MS: an evaluation of matrix effects. Chem. Geol. 225, 121–136. http://dx.doi.org/10.1016/j.chemgeo.2005.09.002.

Rusk, B.G., Reed, M.H., Dilles, J.H., 2008. Fluid-inclusion evidence for magmatic-hydrothermal fluid evolution in the porphyry copper-molybdenum deposit at Butte, Montana. Econ. Geol. 103, 307–333. http://dx.doi.org/10.2113/gsecongeo.103.2.307.

Shafiei, B., Shamanian, G., Mathur, R., Mirnejad, H., 2014. Mo isotope fractionation during hydrothermal evolution of porphyry Cu systems. Mineral. Deposita http://dx.doi.org/10.1007/s00126-014-0537-0.

Siebert, S., Nägler, T.F., Kramers, J.D., 2001. Determination of molybdenum isotope fractionation by double-spike multicollector inductively coupled plasma mass spectrometry. Geochem. Geophys. Geosyst. 2. http://dx.doi.org/10.1029/2000GC000124 (paper number 2000GC000124).

Siebert, C., Nägler, T.F., von Blanckenburg, F., Kramers, J.D., 2003. Molybdenum isotope records as a potential new proxy for paleoceanography. Earth Planet. Sci. Lett. 211, 159–171. http://dx.doi.org/10.1016/S0012-821X(03)00189-4.

Voegelin, A.R., Pettke, T., Greber, N.D., von Niederhäusern, B., Nägler, T.F., 2014. Magma differentiation fractionates Mo isotope ratios: evidence from the Kos Plateau Tuff (Aegean Arc). Lithos 190-191, 440–448. http://dx.doi.org/10.1016/j.lithos.2013.12.016.

Wallmach, T., Hatton, C.J., Droop, G.T.R., 1989. Extreme facies of contact metamorphism developed in calc-silicate xenoliths in the eastern bushveld complex. Can. Mineral. 27, 509–523.

Wen, H., Carignan, J., Cloquet, C., Zhu, X., Zhang, Y., 2010. Isotopic delta values of molybdenum standard reference and prepared solutions measured by MC-ICP-MS: proposition for delta zero and secondary references. J. Anal. At. Spectrom. 25, 716–721. http://dx.doi.org/10.1039/B921060A.

Wieser, M.E., De Laeter, J.R., 2000. Thermal ionization mass spectrometry of molybdenum isotopes. Int. J. Mass Spectrom. 197, 253–261.

Wieser, M.E., de Laeter, J.R., 2003. A preliminary study of isotope fractionation in molybdenites. Int. J. Mass Spectrom. 225, 177–183.

Zhai, D., Liu, J., Wang, J., Yang, Y., Zhang, H., Wang, X., Zhang, Q., Wang, G., Liu, Z., 2014. Zircon U–Pb and molybdenite Re–Os geochronology, and whole–rock geochemistry of the Hashitu molybdenum deposit and host granitoids, Inner Mongolia, NE China. J. Asian Earth Sci. 79, 144–160. http://dx.doi.org/10.1016/j.jseaes.2013.09.008.

Zhu, X.K., Guo, Y., Williams, R.J.P., O'Nions, R.K., Matthews, A., Belshaw, N.S., Canters, G.W., de Waal, E.C., Weser, U., Burges, s.B.K., Salvato, B., 2002. Mass fractionation processes of transition metal isotopes. Earth Planet. Sci. Lett. 200, 47–62. http://dx.doi.org/10.1016/S0012-821X(02)00615-5.